

Spin chain on a metallic surface: Dissipation-induced order vs. Kondo entanglement

Bimla Danu,¹ Matthias Vojta,² Tarun Grover,³ and Fakher F. Assaad¹

¹*Institut für Theoretische Physik und Astrophysik and Würzburg-Dresden Cluster of Excellence ct.qmat, Universität Würzburg, 97074 Würzburg, Germany*

²*Institut für Theoretische Physik und Würzburg-Dresden Cluster of Excellence ct.qmat, Technische Universität Dresden, 01062 Dresden, Germany*

³*Department of Physics, University of California at San Diego, La Jolla, CA 92093, USA*

(Dated: April 4, 2022)

We explore the physics of a spin-1/2 Heisenberg chain with Kondo interaction, J_k , to a two-dimensional electron gas. At weak J_k the problem maps onto a Heisenberg chain locally coupled to a dissipative Ohmic bath. At the decoupled fixed point, the dissipation is a marginally relevant perturbation and drives long-range antiferromagnetic order along the chain. In the dynamical spin structure factor we observe a quadratic low-energy dispersion akin to Landau-damped Goldstone modes. At large J_k Kondo screening dominates, and the spin correlations of the chain inherit the power law of the host metal, akin to a paramagnetic heavy Fermi liquid. In both phases we observe heavy bands near the Fermi energy in the composite-fermion spectral function. Our results, obtained from auxiliary-field quantum Monte Carlo simulations, provide a unique negative-sign-free realization of a quantum transition between an antiferromagnetic metal and a heavy-fermion metal. We discuss the relevance of our results in the context of scanning tunneling spectroscopy experiments of magnetic adatom chains on metallic surfaces.

Introduction. A spin-1/2 antiferromagnetic chain embedded in a higher-dimensional metal, with Kondo coupling J_k between spins and electrons, represents an arena for rich physics. For two-dimensional metals, this relates to scanning tunneling microscopy (STM) experiments, with the ability to build and probe assemblies of magnetic adatoms on surfaces [1–5]. In higher dimensions, $\text{Yb}_2\text{Pt}_2\text{Pb}$ provides a realization of one-dimensional spin chains embedded in a three-dimensional metal [6, 7]. Due to the dimensionality mismatch, such a system remains metallic even for a half-filled conduction band. It can host a variety of phases that include Kondo-breakdown or orbital-selective Mott states [8, 9], heavy-fermion physics in which the magnetic spins, albeit sub-extensive, participate in the Luttinger volume, as well as non-Fermi-liquid states [10]. The understanding of quantum transitions between these states is of considerable interest both experimentally and theoretically.

In this letter, we will consider the above setup for two-dimensional electrons in the presence of a Fermi surface. In the limit of weak Kondo coupling, one can follow the Hertz-Millis approach [11, 12] and perturbatively integrate out the fermions to arrive at an effective description of the spin chain locally coupled to an Ohmic bath [13–17]. As argued in Ref. 17, for an $O(3)$ quantum rotor model coupled to an Ohmic bath, the dissipation is marginally relevant and leads to long-range magnetic ordering along the chain. Hence, unlike in conventional heavy-fermions systems where Ruderman-Kittel-Kasuya-Yosida (RKKY) interactions directly drive magnetic ordering [18, 19], here the ordering is stabilized only by the dissipation. As the Kondo coupling increases, Kondo screening will compete with dissipation-induced ordering. In particular, in the strong-coupling limit, it is expected that the spin-rotation symmetry will be restored in the

chain, and the spin-spin correlations of the chain will inherit the power-law decay of the host metal. The physics of the Heisenberg spin chain on a metallic surface can hence be cast into the flow diagram of Fig. 1(a) where Kondo-singlet formation and dissipation-induced order compete.

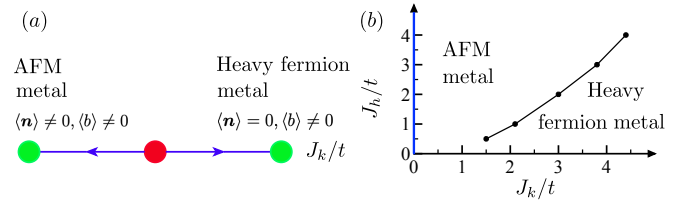


FIG. 1. (a) RG flow diagram as suggested by the QMC data. Green (red) bullets correspond to phases (critical points). We observe an antiferromagnetic order-disorder transition with $\langle n \rangle$ the $O(3)$ order parameter. In both phases Kondo screening, corresponding to a Higgs condensate $\langle b \rangle \neq 0$, is present. (b) Phase diagram in the J_h versus J_k plane as extracted from QMC simulations at $\beta \propto L^z$ with $z = 2$. The blue line at $J_k = 0$ represents the decoupled Heisenberg chain that is unstable to dissipation-induced ordering upon Kondo coupling to the fermions.

Model and Method. Our starting point is the Hamiltonian for a spin-1/2 chain on a metallic surface,

$$\hat{H} = -t \sum_{\langle i,j \rangle} (\hat{c}_i^\dagger \hat{c}_j + \text{H.c.}) + \frac{J_k}{2} \sum_{r=1}^L \hat{c}_r^\dagger \sigma \hat{c}_r \cdot \hat{S}_r + J_h \sum_{r=1}^L \hat{S}_r \cdot \hat{S}_{r+\Delta r}. \quad (1)$$

Here, the summation $\sum_{\langle i,j \rangle}$ runs over nearest neighbors of a square-lattice, $L \times L$, conducting substrate, t

is the hopping matrix element, and $\hat{\mathbf{c}}_i^\dagger = (\hat{c}_{i,\uparrow}^\dagger, \hat{c}_{i,\downarrow}^\dagger)$ is a spinor where $\hat{c}_{i,\uparrow(\downarrow)}^\dagger$ creates an electron at site i with z -component of spin $1/2$ ($-1/2$). J_k is the antiferromagnetic Kondo coupling between spins and conduction electrons, J_h is the antiferromagnetic Heisenberg coupling, $\hat{\mathbf{S}}_r$ are spin-1/2 operators and L is the length of the chain. We consider an array of ad-atoms at an interatomic spacing $\Delta\mathbf{r} = (a, 0)$ with $a = 1$ and periodic boundary conditions are used along the spin chain as well as for the conduction electrons. Translation by $(a, 0)$ is a symmetry of the problem such that crystal momentum \mathbf{k} along the chain is conserved up to a reciprocal lattice vector. This model, including the Heisenberg exchange, is motivated by the STM work of Ref. 1.

In the absence of Kondo coupling and at $J_h \neq 0$, the local moments at low-energies are described by a Luttinger liquid action $\mathcal{S}_{\text{chain}}$. Denoting the fluctuating antiferromagnetic (AFM) order parameter as \mathbf{n} , in this theory $\langle \mathbf{n}(\mathbf{r}, \tau) \cdot \mathbf{n}(\mathbf{0}, 0) \rangle \sim \sqrt{\log(r^2 + \tau^2)} / \sqrt{r^2 + \tau^2}$. Here $r = |\mathbf{r}|$. When $J_k \neq 0$, one may proceed by integrating out the conduction electrons and obtain an action up to second order in J_k as $\mathcal{S} = \mathcal{S}_{\text{chain}} + \mathcal{S}_{\text{diss}}(\mathbf{n})$ with

$$\mathcal{S}_{\text{diss}}(\mathbf{n}) = \frac{J_k^2}{8} \int d\tau d\tau' \sum_{\mathbf{r}, \mathbf{r}'} \mathbf{n}_{\mathbf{r}}(\tau) \chi^0(\mathbf{r} - \mathbf{r}', \tau - \tau') \mathbf{n}_{\mathbf{r}'}(\tau'). \quad (2)$$

where χ^0 is the antiferromagnetic spin susceptibility of the conduction electrons and $\mathcal{S}_{\text{chain}}$ the action of the spin chain. For generic, non-nested two-dimensional electrons at finite density, $\chi^0(\mathbf{r} = 0, \tau) \sim 1/\tau^2$, while $\chi^0(\mathbf{r}, \tau = 0) \sim 1/r^3$. Using power counting, one observes that while the long-range $1/r^3$ spatial decay of χ^0 is irrelevant at the $J_k = 0$ fixed point, the long-range $1/\tau^2$ decay in the time direction is not innocuous, and at the leading order, corresponds to a dissipative Ohmic bath that is marginal in the renormalization-group sense. In fact, as argued in [17], such a dissipative coupling is a marginally relevant operator that triggers long-range order. To avoid the negative-sign-problem we employ a particle-hole-symmetric conduction band such that the Fermi surface is nested. As shown in supplemental material [20] this leads to a multiplicative logarithmic correction to χ^0 : $\chi^0(\mathbf{0}, \tau) \sim \log^2(\tau)/\tau^2$. Therefore, at small J_k , the logarithmic enhancement only increases the tendency for the system to become ordered due to dissipation. A particularity of the nested Fermi surface is a directional dependence of $\chi^0(\mathbf{r}, 0)$ [20]. For a chain along the $(a, 0)$ direction $\chi^0(\mathbf{r}, 0) \sim 1/r^4$. At $J_k \gg J_h, t$ the local moments prefer to form local singlets with the conduction electrons, thereby resulting in a paramagnetic phase.

We simulate the Hamiltonian of Eq. (1) using the auxiliary-field quantum Monte Carlo (AFQMC) [21, 22] implementation of the Algorithms for Lattice Fermions (ALF) [23, 24] library. The model falls in the general category of spin-fermion Hamiltonians [25] that do not suffer

from the sign problem. Our simulations are based on the finite-temperature grand-canonical AFQMC [26, 27]. To reduce finite-size effects we have included an orbital magnetic field of magnitude $B = \Phi_0/L^2$ where Φ_0 is the flux quantum [28].

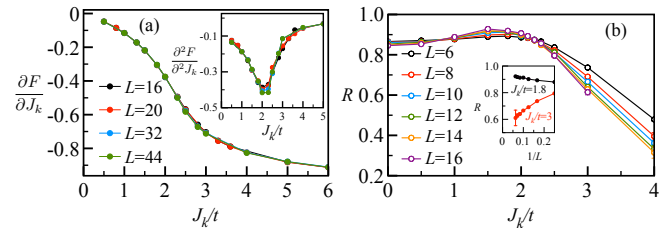


FIG. 2. (a) First derivative of free energy as a function of J_k/t at $\beta t = L$ and $J_h/t = 1$. The inset plots the second derivative of the free energy. (b) Correlation ratio R as a function of J_k/t at $\beta t = L^2/2$ and $J_h/t = 1$. The inset plots R as a function of $1/L$ at $J_k/t = 1.8$ and $J_k/t = 3$.

QMC Results. Given the above considerations, we anticipate an order-disorder transition as a function of J_k . To locate it, we consider $\frac{1}{L} \frac{\partial F}{\partial J_k} = \frac{2}{3L} \sum_{\mathbf{r}} \langle \hat{\mathbf{c}}_{\mathbf{r}}^\dagger \boldsymbol{\sigma} \hat{\mathbf{c}}_{\mathbf{r}} \cdot \hat{\mathbf{S}}_{\mathbf{r}} \rangle$ as a function of J_k as well as $\frac{\partial^2 F}{\partial J_k^2}$ (Fig. 2(a) and inset). As apparent, the data is consistent with a single transition at $J_k^c/t \simeq 2.1$ for $J_h/t = 1$. Next, we consider the spin susceptibility,

$$\chi(\mathbf{k}, i\Omega_m) = \int_0^\beta d\tau \sum_{\mathbf{r}} e^{i(\Omega_m \tau - \mathbf{k} \cdot \mathbf{r})} \langle \hat{S}_{\mathbf{r}}^z(\tau) \hat{S}_{\mathbf{0}}^z(0) \rangle, \quad (3)$$

from which we can define the correlation ratio,

$$R = 1 - \frac{\chi(\mathbf{Q} - \delta\mathbf{k}, 0)}{\chi(\mathbf{Q}, 0)}, \quad (4)$$

where $\mathbf{Q} = (\pi/a, 0)$ corresponds to the antiferromagnetic wave vector and $\delta\mathbf{k}$ to the smallest wave vector on the L -site chain. This correlation ratio scales to unity (zero) for ordered (disordered) states, and at criticality, is a renormalization group invariant quantity. Here, $R = f([J_k - J_k^c] L^{1/\nu}, L^z/\beta, L^{-\omega})$ where ν is the correlation length exponent, z is the dynamical exponent, and ω captures corrections to scaling. Figs. 4 (c) and (d) shows that in the vicinity of the critical point spatial correlations drop off as $1/r$ whereas along the imaginary time, we observe a much slower $1/\sqrt{\tau}$ decay. This suggests a critical exponent $z \simeq 2$. With this in mind, we can compute R adopting a $\beta t = L^2$ scaling such that under the assumption vanishing correlations to scaling, R should show a crossing point as a function of system size at J_k^c . As apparent from Fig. 2(b) R shows a crossing at $J_k^c/t \simeq 2.1$ thus providing a consistency check for our choice of the dynamical exponent. We now discuss the physics at weak, $J_k < J_k^c$, and strong coupling, $J_k > J_k^c$.

For $J_k < J_k^c$, we expect-dissipation induced long-range AFM ordering. As discussed in [20], in this phase one

can decompose the fluctuating AFM field \mathbf{n} as $\mathbf{n}(r, \tau) = (\boldsymbol{\sigma}(r, \tau), \sqrt{1 - \boldsymbol{\sigma}(r, \tau)^2})$ where the ordering is assumed along the \hat{z} direction. The low-energy action for the transverse fluctuations $\boldsymbol{\sigma}$ has dynamical exponent $z = 2$, and is given by $\mathcal{S}_0(\boldsymbol{\sigma}) = \frac{\Gamma}{2} \int d\tau d\tau' dr \frac{\boldsymbol{\sigma}(r, \tau) \cdot \boldsymbol{\sigma}(r, \tau')}{(\tau - \tau')^2} + \frac{\rho_s}{2} \int d\tau dr (\partial_r \boldsymbol{\sigma}(r, \tau))^2$. This implies that while the n^z correlations are long-ranged in both space and time, the correlations of $\boldsymbol{\sigma}$ are given as: $\langle \boldsymbol{\sigma}(r, \tau) \cdot \boldsymbol{\sigma}(r, 0) \rangle \sim 1/\sqrt{\tau}$, while $\langle \boldsymbol{\sigma}(0, \tau) \cdot \boldsymbol{\sigma}(r, \tau) \rangle \sim 1/r$.

On the numerical front, at $J_k/t = 1.8 < J_k^c/t$, we observe a slight increase in the correlation ratio (Fig. 2(b) inset) thus hinting to the onset of long-range order, but as J_k decreases further no sign of long-range order on our finite lattice sizes is apparent. To understand this apparent lack of ordering, we can switch off the Kondo screening and retain only local dissipation, corresponding to Eq. (2) with $\chi^0(\mathbf{r}, \tau) \propto \delta_{\mathbf{r}, \mathbf{0}}/\tau^2$. For this bosonic model stochastic series approaches for retarded interactions [29, 30] can be used to investigate this model with unprecedented precision [17]. It was shown in Ref. [17] that the marginally relevant nature of the Ohmic dissipation at the LL critical point requires lattice sizes $L \ll L_c \propto e^{\xi/J_k^2}$ to detect long-range order.

For $L \lesssim L_c$ one observes crossover phenomena characterized by a $1/r$ decay of the real space spin-spin correlations and breakdown of Lorentz symmetry. Our understanding is that our data falls in this crossover regime, and that for $r \ll L_c$ it can be accounted for by

$$C(r, \tau) \propto \begin{cases} \frac{1}{\sqrt{r^2 + \tau^{2/z}}} & \tau \ll \frac{1}{\Delta} \\ \frac{e^{-\Delta\tau}}{\sqrt{r^2 + \Delta^{-2/z}}} & \tau \gg \frac{1}{\Delta} \end{cases} \quad (5)$$

on an L -site lattice. Here $C(r, \tau) = e^{i\mathbf{Q} \cdot \mathbf{r}} \langle \hat{S}_{\mathbf{r}}^z(\tau) \hat{S}_{\mathbf{0}}^z(0) \rangle$ and $\Delta \propto (\frac{2\pi}{L})^z$ corresponds to the finite-size gap. At $J_k/t = 0.5$, far from the critical point, Fig. 4 plots $C(r, 0)$ (a) as well as $C(0, \tau)$ (b). The real-space equal-time decay is consistent with a $1/r$ law. Along the imaginary time we observe crossover phenomena: While at short times, $\tau t \lesssim L$, the temporal decay is consistent with Eq. (5) at $z \simeq 1$ akin to the Heisenberg model, we observe at large τ a breakdown of Lorentz invariance with $C(0, \tau)$ decaying substantially slower than $1/\tau$. In the infinite-size limit, we foresee that both the real-space and imaginary-time correlations will level off to show long-ranged correlations, albeit with a very small local moment.

The breakdown of Lorentz invariance is equally apparent in the data of Fig. 3. The Ansatz of Eq. (5) leads a structure factor $S(\mathbf{Q}) = \frac{1}{\beta} \sum_{\Omega_m} \chi(\mathbf{Q}, i\Omega_m)$ that is independent on the dynamical exponent and as for the Heisenberg chain diverges as $\log(L)$. The size scaling in the crossover regime (Fig. 3(a)) does not show marked differences from the Heisenberg limit. As noted in Ref. [17] and seen in Fig. 3(a), coupling to the bath reduces the magnitude of the equal time spin-correlations.

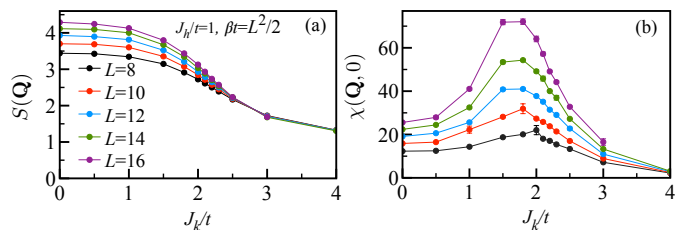


FIG. 3. (a) Static spin structure factor $S(\mathbf{Q})$ along the spin chain as a function of J_k/t for given L at $J_h/t = 1$ and $\beta t = L^2/2$. (b) Correspondingly, spin susceptibility $\chi(\mathbf{Q}, 0)$ as a function of J_k/t .

On the other hand, the susceptibility, $\chi(\mathbf{Q}, 0)$ shows marked differences as a function of J_k . In Fig. 3(b) we consider the scaling $\beta t = L^2/2$. In the Heisenberg limit this leads to $\chi(\mathbf{Q}, 0) \propto L$ and a marked deviation from this law is observed in the crossover regime. For $z = 2$ akin to the critical point, $J_k^c/t \simeq 2.1$, the Ansatz of Eq. (5) yields $\chi(\mathbf{Q}, 0) \propto L^2$. This scaling law is supported by the data thus confirming $z \simeq 2$ at criticality.

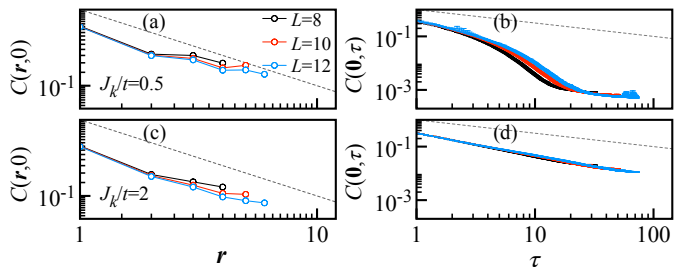


FIG. 4. Space and time correlation functions $C(\mathbf{r}, \tau)$ at $\beta t = L^2$ and $J_h/t = 1$. (a) $C(\mathbf{r}, 0)$ at $J_k/t = 0.5$. (b) $C(\mathbf{0}, \tau)$ at $J_k/t = 0.5$. (c) $C(\mathbf{r}, 0)$ at $J_k/t = 0.5$. (d) $C(\mathbf{0}, \tau)$ at $J_k/t = 2$. The dashed grey lines denote the $1/r$ ((a) and (c)) and $1/\sqrt{\tau}$ ((b) and (d)) power laws.

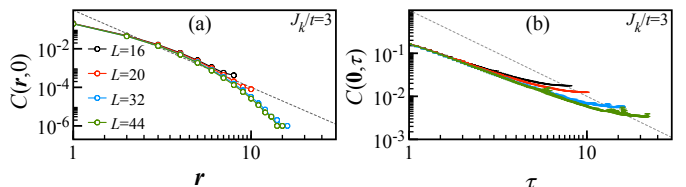


FIG. 5. Space and time correlation functions along the spin chain in the Kondo-screened phase at $J_h/t = 1$, $J_k/t = 3$ and $\beta t = L$. (a) $C(\mathbf{r}, 0)$. The dashed grey line indicates a $1/r^4$ power law. (b) $C(\mathbf{0}, \tau)$. The dashed grey line indicates a $1/\tau^2$ law. Both power laws in time and in space are observed in the large- N limit (see Ref. [20]).

At $J_k > J_k^c$ we are in a Kondo screened phase that can be understood within a large- N mean field theory presented in Ref. [20]. In this phase, the spin-spin correlations inherit the asymptotic behavior of the conduction electrons and fall off as $1/r^4$ in space and as $1/\tau^2$ in

imaginary time. In particular, Figs. S2 and S3 of Ref. 20 plot the space- and time-displaced correlation functions within the large- N approximation and confirm the above. The QMC data of Fig. 5 is consistent with this expectation.

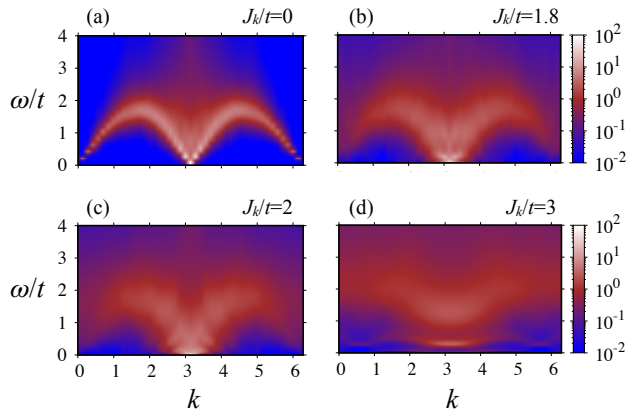


FIG. 6. $S(k, \omega)$ as a function of energy ω/t and momentum k along the spin chain at $\beta t = L = 44$ and $J_h/t = 1$.

Using the ALF [24] implementation of the maximum Entropy method [31, 32] we compute the dynamical spin structure factor $S(\mathbf{k}, \omega) = \frac{\text{Im}\chi(\mathbf{k}, \omega + i0^+)}{1 - e^{-\beta\omega}}$. Fig. 6(a) plots this quantity for the Heisenberg model. The data shows the well known two spinon continuum [33–35]. At finite Kondo couplings (Figs. 6(b)–(c)), the two-spinon continuum is still apparent at elevated energies. However the low-energy bound shows a marked deviation from the linear dispersion and is very suggestive of a $\omega \propto k^2$ law. In fact, a field theory presented in Ref. 20 as well as a large- S calculation [17] of a Heisenberg chain locally coupled to an Ohmic bath confirms that dissipation stabilizes long-range order and that the lower bound of the dispersion relation follows an $\omega \propto k^2$ law akin to Landau-damped Goldstone modes. Our dynamical data bears similarities with spinon binding as observed in KCuF_3 [36] and corresponding to a dimensional crossover [37]. In the present case, the elevated-energy spectrum shows the two-spinon continuum while the low energy to corresponds the spin-wave excitations of the Heisenberg chain coupled to an Ohmic bath [20]. Finally, in the Kondo-screened phase at $J_k/t = 3$ see Fig. 6 (d) the low-lying spectral weight is depleted.

We now turn our attention to Kondo screening and heavy-fermion physics. Consider the composite-fermion operator $\hat{\psi}_{\mathbf{r},\sigma}^\dagger = 2 \sum_{\sigma'} \hat{c}_{\mathbf{r},\sigma'}^\dagger \sigma_{\sigma',\sigma} \cdot \hat{\mathbf{S}}_{\mathbf{r}}$ [38–40]. In the large- N limit this quantity picks up the Higgs condensate or hybridization matrix element [20], characteristic of Kondo screening [41]. Here we compute the spectral function $A_\psi(\mathbf{k}, \omega) = -\text{Im}G_\psi^{\text{ret}}(\mathbf{k}, \omega)$ with $G_\psi^{\text{ret}}(\mathbf{k}, \omega) = -i \int_0^\infty dt e^{i\omega t} \sum_\sigma \langle \{ \hat{\psi}_{\mathbf{k},\sigma}(t), \hat{\psi}_{\mathbf{k},\sigma}^\dagger(0) \} \rangle$, representing the conduction-electron T matrix. Figs. 7(a)–(b) shows flat (i.e heavy) bands in the vicinity of the

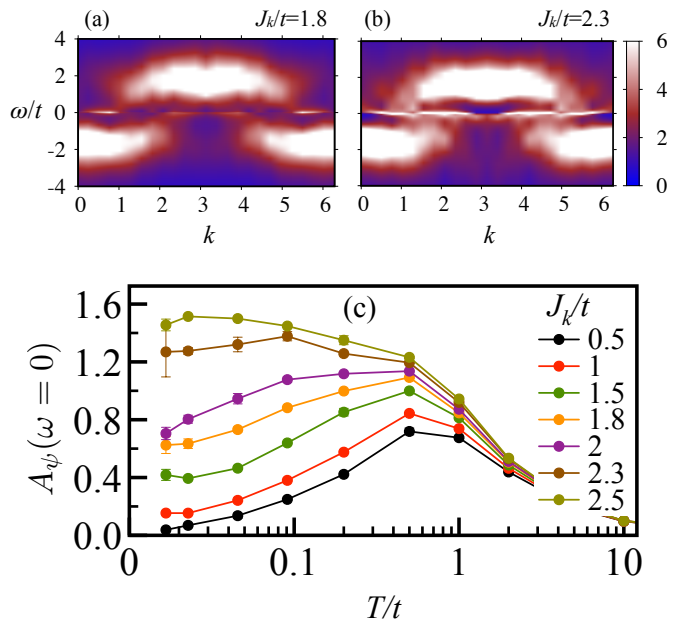


FIG. 7. Spectral function of the composite-fermion operator $A_\psi(k, \omega)$ on an $L = 24$ lattice at $\beta t = 48$ (a) in the ordered phase and (b) in the Kondo-screened phase. (c) Local zero-bias signal $A_\psi(\omega = 0)$ as a function of temperature T/t at $L = 44$ and for various values of J_k/t in the ordered and disordered phases.

Fermi energy, both below and above the critical point $J_k^c/t \simeq 2.1$. In Fig. 7(c) we plot $A_\psi(\omega) = \frac{1}{L} \sum_{\mathbf{k}} A_\psi(\mathbf{k}, \omega)$ as a function of temperature and J_k . To avoid analytical continuation, we use the relation $A_\psi(\omega = 0) \simeq (1/\pi)\beta G_\psi(\tau = \beta/2)$. Confirming the \mathbf{k} -dependent data, we see that this quantity never vanishes at low temperatures in both phases. Hence, the data supports the point of view that Kondo screening is active in the dissipation-induced ordered phase. It is interesting to note that the temperature dependence of $A_\psi(\omega = 0)$ differs in both phases. While it grows and saturates in the Kondo-screened phase, it shows a maximum in the ordered phase. Such a behavior can be understood in terms of the onset of ordering that opens a pseudogap in the spectral function, see Ref. 20. $A_\psi(\omega = 0)$ is an important quantity since it provides a link to STM experiments. In fact, it corresponds to the zero bias signal $dI_t/dV(V = 0)$ for tunneling processes between the tip and the substrate that involve intermediate excited states of the localized orbital. In the experiments described in Refs. [1, 42] and modelled in Ref. [5] J_k can be tuned by changing the width of the Cu_2N islands between the Co adatoms and $\text{Cu}(100)$ surface. Provided that the chains are long enough, our observation of distinct temperature behaviors of $A_\psi(\omega = 0)$ in the two phases provides a means to experimentally distinguish them.

Conclusions. The physics of the Heisenberg chain coupled to two-dimensional electrons can be understood by

the competition between dissipation and Kondo screening. Not unlike the competition between the RKKY interaction and Kondo screening, the Kondo coupling triggers both effects but at different energy scales.

At weak coupling dissipation dominates, and the chain develops long-range antiferromagnetic order. Since the coupling to the Ohmic bath is marginally relevant [17], system sizes exceeding our achievable lattices are required to unambiguously detect the order. As a consequence our data below the critical point are dominated by a crossover regime characterized by the absence of Lorentz invariance as seen in Ref. 17. In fact, the tendency towards ordering on small lattices can be enhanced by considering the XXZ (as opposed to Heisenberg) chain in its Luttinger-liquid phase. Here the transverse spin operator acquires a scaling dimension smaller than $1/2$ such that the coupling to the Ohmic bath becomes relevant. In Ref. 20 we have verified that the XXZ chain indeed leads to a stronger tendency towards ordering. At strong coupling, Kondo screening dominates, leading to a paramagnetic phase. Here, the spin-spin correlations inherit the power-law decay of the host metal. Aspects of this phase diagram have been put forward based on analytical considerations in Ref. 43.

The composite-fermion spectral function reveals a heavy band in both phases. Hence, in the ordered phase Kondo screening coexists with dissipation-induced ordering. In the disordered phase, the notion of heavy Fermi liquid can be made precise by invoking the Luttinger theorem that relates the size of the Fermi surface to the count of its constituents. Since our model preserves translation invariance along the chain, it can be thought of as a one-dimensional model with a unit cell that contains L conduction electrons and single spin- $1/2$ local moment. With this formulation, one can now apply Oshikawa's proof of Luttinger theorem in the context of Kondo lattices [44], and show that the volume of the Fermi surface includes the local moments, assuming that the system is described by a Fermi liquid at low energies. An explicit calculation is presented in Ref. 20.

Our model provides a unique negative-sign-free realization of a Hertz-Millis-type transition between antiferromagnetic and paramagnetic heavy-fermion metals. To avoid the negative-sign problem we have to consider a particle-hole symmetric conduction band with inherent nesting instabilities. Nevertheless, we expect that the our broad conclusions, including the global structure of the phase diagram, hold for a generic two-dimensional Fermi surface. In the latter case, the spin-spin correlations of the host metal decay as $1/r^3$ and as $1/\tau^2$ in space and time, respectively. Since the $1/r^3$ decay is an irrelevant perturbation at the decoupled fixed point, we expect dissipation-induced ordering to occur generically at small J_k . Our numerical data suggests that the transition in Fig. 1 is characterized by a dynamical exponent $z \simeq 2$. A detailed understanding of the transition, both

on the numerical and analytical fronts, remains for future work.

FFA thanks D. Luitz and M. Weber for discussions on the dissipative Heisenberg chain. The authors gratefully acknowledge the Gauss Centre for Supercomputing e.V. (www.gauss-centre.eu) for providing computing time on the GCS Supercomputer SUPERMUC-NG at Leibniz Supercomputing Centre (www.lrz.de). The research has been supported by the Deutsche Forschungsgemeinschaft through grant number AS 120/14-1 (FFA), the Würzburg-Dresden Cluster of Excellence on Complexity and Topology in Quantum Matter - ct.qmat (EXC 2147, project-id 390858490) (FFA and MV), and SFB 1143 (project-id 247310070) (MV). TG is supported by the National Science Foundation under Grant No. DMR-1752417, and as an Alfred P. Sloan Research Fellow. FFA and TG thank the BaCaTeC for partial financial support.

-
- [1] R. Toskovic, R. van den Berg, A. Spinelli, I. S. Eliens, B. van den Toorn, B. Bryant, J. S. Caux, and A. F. Otte, *Nat. Phys.* **12**, 656 (2016).
 - [2] D. J. Choi, R. Robles, S. Yan, J. A. J. Burgess, S. Rolf-Pissarczyk, J. P. Gauyacq, N. Lorente, M. Ternes, and L. Sebastian, *Nano Lett.* **17**, 6203 (2017).
 - [3] M. Moro-Lagares, R. Korytr, M. Piantek, R. Robles, N. Lorente, J. I. Pascual, M. R. Ibarra, and D. Serrate, *Nat. Commun.* **10**, 2211 (2019).
 - [4] D.-J. Choi, N. Lorente, J. Wiebe, K. von Bergmann, A. F. Otte, and A. J. Heinrich, *Rev. Mod. Phys.* **91**, 041001 (2019).
 - [5] B. Danu, F. F. Assaad, and F. Mila, *Phys. Rev. Lett.* **123**, 176601 (2019).
 - [6] L. S. Wu, W. J. Gannon, I. A. Zaliznyak, A. M. Tsvetlik, M. Brockmann, J.-S. Caux, M. S. Kim, Y. Qiu, J. R. D. Copley, G. Ehlers, A. Podlesnyak, and M. C. Aronson, *Science* **352**, 1206 (2016).
 - [7] W. J. Gannon, I. A. Zaliznyak, L. S. Wu, A. E. Feiguin, A. M. Tsvetlik, F. Demmel, Y. Qiu, J. R. D. Copley, M. S. Kim, and M. C. Aronson, *Nature Communications* **10**, 1123 (2019).
 - [8] M. Vojta, *J. Low Temp. Phys.* **161**, 203 (2010).
 - [9] B. Danu, M. Vojta, F. F. Assaad, and T. Grover, *Phys. Rev. Lett.* **125**, 206602 (2020).
 - [10] L. Classen, I. Zaliznyak, and A. M. Tsvetlik, *Phys. Rev. Lett.* **120**, 156404 (2018).
 - [11] J. A. Hertz, *Phys. Rev. B* **14**, 1165 (1976).
 - [12] A. J. Millis, *Phys. Rev. B* **48**, 7183 (1993).
 - [13] P. Werner, M. Troyer, and S. Sachdev, *J. Phys. Soc. Jpn* **74**, 67 (2005).
 - [14] P. Werner, K. Völker, M. Troyer, and S. Chakravarty, *Phys. Rev. Lett.* **94**, 047201 (2005).
 - [15] M. A. Cazalilla, F. Sols, and F. Guinea, *Phys. Rev. Lett.* **97**, 076401 (2006).
 - [16] Z. Yan, L. Pollet, J. Lou, X. Wang, Y. Chen, and Z. Cai, *Phys. Rev. B* **97**, 035148 (2018).
 - [17] M. Weber, D. J. Luitz, and F. F. Assaad, [arXiv:2112.0212](https://arxiv.org/abs/2112.0212) (2021).
 - [18] M. A. Ruderman and C. Kittel, *Phys. Rev.* **96**, 99 (1954).

- [19] K. Yosida, *Phys. Rev.* **106**, 893 (1957).
- [20] See Supplemental Material, which includes Refs. [45, 46], for logarithmic correction to power law decay, stability of AFM phase, mean field calculation, Luttinger theorem, XXZ spin chain, and for other QMC results.
- [21] R. Blankenbecler, D. J. Scalapino, and R. L. Sugar, *Phys. Rev. D* **24**, 2278 (1981).
- [22] S. R. White, D. J. Scalapino, R. L. Sugar, E. Y. Loh, J. E. Gubernatis, and R. T. Scalettar, *Phys. Rev. B* **40**, 506 (1989).
- [23] M. Bercx, F. Goth, J. S. Hofmann, and F. F. Assaad, *SciPost Phys.* **3**, 013 (2017).
- [24] ALF Collaboration, F. F. Assaad, M. Bercx, F. Goth, A. Götz, J. S. Hofmann, E. Huffman, Z. Liu, F. Parisen Toldin, J. S. E. Portela, and J. Schwab, [arXiv:2012.11914](https://arxiv.org/abs/2012.11914) (2020).
- [25] T. Sato, F. F. Assaad, and T. Grover, *Phys. Rev. Lett.* **120**, 107201 (2018).
- [26] F. F. Assaad and H. G. Evertz, in *Computational Many-Particle Physics*, Lecture Notes in Physics, Vol. 739, edited by H. Fehske, R. Schneider, and A. Weiße (Springer, Berlin Heidelberg, 2008) pp. 277–356.
- [27] S. Capponi and F. F. Assaad, *Phys. Rev. B* **63**, 155114 (2001).
- [28] F. F. Assaad, *Phys. Rev. B* **65**, 115104 (2002).
- [29] M. Weber, F. F. Assaad, and M. Hohenadler, *Phys. Rev. Lett.* **119**, 097401 (2017).
- [30] M. Weber, [arXiv:2108.01131](https://arxiv.org/abs/2108.01131) [arXiv:2108.01131](https://arxiv.org/abs/2108.01131).
- [31] A. Sandvik, *Phys. Rev. B* **57**, 10287 (1998).
- [32] K. S. D. Beach, [arxiv:0403055](https://arxiv.org/abs/0403055) (2004).
- [33] J. des Cloizeaux and J. J. Pearson, *Phys. Rev.* **128**, 2131 (1962).
- [34] G. Müller, H. Thomas, H. Beck, and J. C. Bonner, *Phys. Rev. B* **24**, 1429 (1981).
- [35] J.-S. Caux and J. M. Maillet, *Phys. Rev. Lett.* **95**, 077201 (2005).
- [36] B. Lake, D. A. Tennant, C. D. Frost, and S. E. Nagler, *Nature Materials* **4**, 329 (2005).
- [37] M. Raczkowski and F. F. Assaad, *Phys. Rev. B* **88**, 085120 (2013).
- [38] T. A. Costi, *Phys. Rev. Lett.* **85**, 1504 (2000).
- [39] L. Borda, L. Fritz, N. Andrei, and G. Zaránd, *Phys. Rev. B* **75**, 235112 (2007).
- [40] M. Raczkowski and F. F. Assaad, *Phys. Rev. Lett.* **122**, 097203 (2019).
- [41] B. Danu, Z. Liu, F. F. Assaad, and M. Raczkowski, *Phys. Rev. B* **104**, 155128 (2021).
- [42] A. Spinelli, M. Gerrits, R. Toskovic, B. Bryant, M. Ternes, and A. F. Otte, *Nat. Commun.* **6**, 10046 (2015).
- [43] A. M. Lobos, M. A. Cazalilla, and P. Chudzinski, *Phys. Rev. B* **86**, 035455 (2012).
- [44] M. Oshikawa, *Phys. Rev. Lett.* **84**, 3370 (2000).
- [45] H. Tsunetsugu, M. Sigrist, and K. Ueda, *Rev. Mod. Phys.* **69**, 809 (1997).
- [46] A. Luther and I. Peschel, *Phys. Rev. B* **12**, 3908 (1975).

Supplemental Material for: Spin chain on a metallic surface: Dissipation-induced order vs. Kondo entanglement

Bimla Danu, Matthias Vojta, Tarun Grover, and Fakher F. Assaad

LOGARITHMIC CORRECTION TO HERTZ-MILLIS ACTION DUE TO NESTED FERMI SURFACE

The spin-susceptibility $\chi^0(\mathbf{r}, \tau)$ of non-interacting conduction electrons is proportional to $\langle \mathbf{c}_\mathbf{r}^\dagger(\tau) \boldsymbol{\sigma} \mathbf{c}_\mathbf{r}(\tau) \cdot \mathbf{c}_\mathbf{0}^\dagger(0) \boldsymbol{\sigma} \mathbf{c}_\mathbf{r}(0) \rangle$. As discussed in the main text, the important contribution to the Hertz-Millis action comes only from $\chi^0(\mathbf{r} = 0, \tau)$. A simple calculation using Wick's theorem shows that $\chi^0(\mathbf{r} = 0, \tau) \sim I^2$ where

$$I = \int_{k_x, k_y \in \text{F.S.}} dk_x dk_y e^{-\tau(\cos k_x + \cos k_y)} \quad (\text{S1})$$

where $k_x, k_y \in \text{F.S.}$ means that k_x, k_y are inside the Fermi surface of the square-lattice nearest-neighbor tight-binding model at half-filling, i.e., the momenta (k_x, k_y) are occupied at $T = 0$. Since the Fermi surface consists of flat portions at angles $\pm\pi/4$, it is convenient to consider the integral I in a rotated coordinate system, $k'_x = (k_x + k_y)/\sqrt{2}$, $k'_y = (-k_x + k_y)/\sqrt{2}$. Utilizing the symmetry of the integrand and rescaling the variables, the integral now becomes

$$I = 8 \int_0^{\pi/2} dk'_x \int_0^{\pi/2} dk'_y e^{-\tau \cos k'_x \cos k'_y} \quad (\text{S2})$$

Since we are interested in the limit $\tau \gg 1$, we can evaluate the above integral using the saddle point. There are two distinct saddle points: the first arises when $k'_x = \pi/2$ and k'_y is not close to $\pi/2$ – these are the boundaries of the Fermi surface that *exclude* the four corner points $(k_x, k_y) = (\pm\pi, 0), (0, \pm\pi)$ of the diamond in original (k_x, k_y) coordinate system. The second set of saddles precisely correspond to these four corner points. These two set of saddle points yield qualitatively different contribution to I , which we denote by I_1 and I_2 respectively.

Let us first consider contribution to from saddles along $(k'_x, k'_y) = (\pi/2, k'_y)$ where k'_y is not close to $\pi/2$. There will be identical contribution from saddles $(k'_x, k'_y) = (k'_x, \pi/2)$ with k'_x not close to $\pi/2$. Close to these saddles, we can write $k'_x = \pi/2 - x$, so that the contribution I_1 to the integral is approximately given by

$$I_1 \sim \int_0^{c_1} dx \int_0^{\pi/2 - c_2} dk'_y e^{-\tau \sin x \cos k'_y} \quad (\text{S3})$$

where $c_1 \ll 1$ is a small number, and $c_2 = O(1)$. The precise values of c_1, c_2 are irrelevant for asymptotic analysis. Since $c_1 \ll 1$, we can expand $\sin(x) \sim x$, and perform the integral over x leading to $I_1 \sim \int_0^{\pi/2 - c_2} dk'_y \frac{1}{\tau \cos k'_y}$. The integral over k'_y converges and yields an $O(1)$ prefactor because by construction, k'_y is never close to $\pi/2$. Therefore, $I_1 \sim 1/\tau$.

Next, consider I_2 , i.e., contribution to I from $(k'_x, k'_y) \approx (\pi/2, \pi/2)$. Writing $k'_x = \pi/2 - x$, $k'_y = \pi/2 - y$, where $x, y \ll 1$, one finds

$$I_2 \sim \int_0^a dx \int_0^a dy e^{-\tau xy} \sim \int_0^a dy \left(\frac{1 - e^{-a\tau y}}{\tau y} \right) \quad (\text{S4})$$

where $a \lesssim 1$ is some constant. Since $\tau \gg 1$, the integrand for the integral over y has two regimes, the first corresponding to $y \lesssim 1/(\tau a)$ and the other $y \gtrsim 1/(\tau a)$. Therefore, we split the integral as

$$I_2 \sim \int_0^{1/(\tau a)} dy \left(\frac{1 - e^{-a\tau y}}{\tau y} \right) + \int_{1/(\tau a)}^a dy \left(\frac{1 - e^{-a\tau y}}{\tau y} \right) \equiv I_{2,A} + I_{2,B} \quad (\text{S5})$$

$I_{2,A}$ is given by

$$I_{2,A} \sim \int_0^{1/(\tau a)} dy \left(\frac{1 - e^{-a\tau y}}{\tau y} \right) \sim 1/\tau \quad (\text{S6})$$

where we have obtained the asymptotic dependence by simply Taylor expanding the integrand, which is allowed because in the range of the integral, $y \ll 1$ (since $1/(\tau a) \ll 1$). In contrast, the leading contribution to $I_{2,B}$ is

$$I_{2,B} \sim \int_{1/(\tau a)}^a dy \left(\frac{1 - e^{-a\tau y}}{\tau y} \right) \sim \frac{1}{\tau} \log(a^2 \tau) \sim \frac{\log(\tau)}{\tau} \quad (S7)$$

Combining everything, at the leading order, $I \sim I_1 + I_2 \sim \frac{\log(\tau)}{\tau}$. Therefore, the leading term in the Hertz-Millis action is proportional to $J_k^2 \int d\tau d\tau' \sum_{\mathbf{r}} \frac{\log^2(\tau - \tau')}{(\tau - \tau')^2} \mathbf{n}_{\mathbf{r}}(\tau) \cdot \mathbf{n}_{\mathbf{r}}(\tau')$, i.e., compared to the case of non-nested Fermi surface, one obtains a multiplicative logarithmic correction.

SPIN AUTOCORRELATIONS FOR A NESTED FERMI SURFACE

For a generic, non-nested Fermi surface in two spatial dimensions, the AFM correlations decay as: $\langle \mathbf{n}(\mathbf{r}) \cdot \mathbf{n}(\mathbf{0}) \rangle \sim 1/r^3$. However, as discussed in the main text, in the paramagnetic phase of our model, we find that the AFM correlations both for the spin-chain and for the conduction electrons decay as: $\langle \mathbf{n}(\mathbf{r}) \cdot \mathbf{n}(\mathbf{0}) \rangle \sim 1/r^4$ when $\mathbf{r} = r(1, 0)$ lies along the direction of the chain. The change in the power-law compared to a generic Fermi surface is a consequence of the nested Fermi surface, and we provide a brief derivation here.

Using Wick's theorem, $\langle \mathbf{n}(\mathbf{r}) \cdot \mathbf{n}(\mathbf{0}) \rangle \sim \langle c_{\mathbf{r},\sigma}^\dagger c_{\mathbf{r},\sigma} \rangle^2 \sim \left(\frac{1}{V} \sum_{\mathbf{k}} n_F(k_x, k_y) e^{i\mathbf{k} \cdot \mathbf{r}} \right)^2$ where $V = L^2$ is the total system size and n_F is the Fermi function at $T = 0$. Orienting the axes so that the filled Fermi sea corresponds to $k_x \in (-\pi/\sqrt{2}, -\pi/\sqrt{2})$, $k_y \in (-\pi/\sqrt{2}, -\pi/\sqrt{2})$, one may now exploit the square shape of the corresponding Fermi surface to decompose n_F as $n_F(k_x, k_y) = f(k_x)f(k_y)$ where $f(k) = 1$ for $k \in (-\pi/\sqrt{2}, -\pi/\sqrt{2})$ and $f(k) = 0$ otherwise. With this coordinate choice, $\mathbf{r} = (\mathbf{x} + \mathbf{y})/\sqrt{2}$. Therefore, one finds

$$\langle \mathbf{n}(\mathbf{r}) \cdot \mathbf{n}(\mathbf{0}) \rangle \sim (g(r))^4 \quad (S8)$$

where $g(r) = \sum_{\mathbf{k}} f(k) e^{i\mathbf{k} \cdot \mathbf{r}} / L$. One now recognizes that $g(r)$ precisely corresponds to the single-particle Green's function for a 1d system with Fermi points at $\pm\pi/\sqrt{2}$, and therefore, $g(r) \sim 1/r$. Thus, one obtains the result seen in our numerics, namely, $\langle \mathbf{n}(\mathbf{r}) \cdot \mathbf{n}(\mathbf{0}) \rangle \sim 1/r^4$. In passing, we note that if \mathbf{r} instead makes a $\pi/4$ angle to the spin-chain, then following the same steps, one finds that $\langle \mathbf{n}(\mathbf{r}) \cdot \mathbf{n}(\mathbf{0}) \rangle \sim 1/r^2$.

STABILITY OF ORDERING FOR A DISSIPATIVE SPIN CHAIN

To gain insight into the stability of magnetic excitations on the spin chain in the presence of dissipative Kondo coupling, let us first consider a one dimensional system with the following imaginary-time non-linear sigma action for an $O(3)$ order parameter \mathbf{n} :

$$\mathcal{S}_{\text{diss}}(\mathbf{n}) = \frac{\Gamma}{2} \int d\tau d\tau' dr \frac{\mathbf{n}(r, \tau) \cdot \mathbf{n}(r, \tau')}{(\tau - \tau')^2} + \frac{\rho_s}{2} \int d\tau dr (\partial_\tau \mathbf{n}(r, \tau))^2 + (\partial_r \mathbf{n}(r, \tau))^2, \quad (S9)$$

where $\mathbf{n}(r, \tau) \cdot \mathbf{n}(r, \tau) = 1$ and Γ is the strength of the dissipation. Let us assume that the $O(3)$ symmetry is spontaneously broken down to $O(2)$ with the order-parameter pointing along the \hat{z} direction. One may then parameterize \mathbf{n} as: $\mathbf{n}(r, \tau) = \left(\boldsymbol{\sigma}(r, \tau), \sqrt{1 - \boldsymbol{\sigma}(r, \tau)^2} \right)$ where $\boldsymbol{\sigma}$ is a two-component vector that captures the transverse fluctuations of \mathbf{n} . Assuming $|\boldsymbol{\sigma}(r, \tau)| \ll 1$, one may then obtain the effective action $\mathcal{S}_{\text{diss}}(\boldsymbol{\sigma})$ in the putative symmetry-broken phase. One finds $\mathcal{S}_{\text{diss}}(\boldsymbol{\sigma}) = \mathcal{S}_0(\boldsymbol{\sigma}) + \mathcal{S}_1(\boldsymbol{\sigma}) + \dots$ where

$$\mathcal{S}_0(\boldsymbol{\sigma}) = \frac{\Gamma}{2} \int d\tau d\tau' dr \frac{\boldsymbol{\sigma}(r, \tau) \cdot \boldsymbol{\sigma}(r, \tau')}{(\tau - \tau')^2} + \frac{\rho_s}{2} \int d\tau dr (\partial_r \boldsymbol{\sigma}(r, \tau))^2, \quad (S10)$$

$$\mathcal{S}_1(\boldsymbol{\sigma}) = \frac{\Gamma}{8} \int d\tau d\tau' dr \frac{\boldsymbol{\sigma}^2(r, \tau) \cdot \boldsymbol{\sigma}^2(r, \tau')}{(\tau - \tau')^2} + \frac{\rho_s}{2} \int d\tau dr (\boldsymbol{\sigma}(r, \tau) \cdot \partial_r \boldsymbol{\sigma}(r, \tau))^2, \quad (S11)$$

and ‘...’ denotes higher order terms that are less relevant than $\mathcal{S}_0(\boldsymbol{\sigma})$ and $\mathcal{S}_1(\boldsymbol{\sigma})$. The action $\mathcal{S}_0(\boldsymbol{\sigma})$ is invariant under the following scaling transformation: $r \rightarrow \lambda r, \tau \rightarrow \lambda^2 \tau, \boldsymbol{\sigma}(r, \tau) \rightarrow \boldsymbol{\sigma}(r, \tau)/\sqrt{\lambda}$. On the other hand, under the same scaling transformation, $\mathcal{S}_1(\boldsymbol{\sigma}) \rightarrow \mathcal{S}_1(\boldsymbol{\sigma})/\lambda$, and therefore, $\mathcal{S}_1(\boldsymbol{\sigma})$ is irrelevant at the RG fixed point governed by $\mathcal{S}_0(\boldsymbol{\sigma})$. Terms such as $\int d\tau dr (\partial_\tau \boldsymbol{\sigma}(r, \tau))^2$ and $\int d\tau dr (\boldsymbol{\sigma} \cdot \partial_\tau \boldsymbol{\sigma})^2$ are even more irrelevant at this fixed point. Therefore, the low-energy theory in the symmetry-broken phase is given by $\mathcal{S}_0(\boldsymbol{\sigma})$, which has dynamical critical exponent $z = 2$ and

corresponds to a Landau-damped Goldstone boson. Irrelevancy of interactions between damped Goldstone modes, such as the term $S_1(\boldsymbol{\sigma})$, indicates that the ordered phase is stable against fluctuations. In contrast, in the absence of the dissipative term in Eq. (S9), i.e. when $\Gamma = 0$, the interactions between the Goldstone modes would be marginal at the leading order, and lead to logarithmic divergence in various quantities, in accordance with Mermin-Wagner theorem. Dissipation alters the scaling dimension of the Goldstone mode, $\boldsymbol{\sigma}$, and obviates Mermin-Wagner theorem.

Another related approach to confirm the stability of the ordered phase is via calculating the reduction in the order parameter due to fluctuations. The magnitude m of the order parameter is $m = \sqrt{1 - \langle \boldsymbol{\sigma}(r, \tau)^2 \rangle} \approx 1 - \langle \boldsymbol{\sigma}(r, \tau)^2 \rangle / 2$. Therefore, at the leading order, the reduction in the order parameter approximately equals $\langle \boldsymbol{\sigma}(r, \tau)^2 \rangle / 2 \sim \int dk d\Omega \frac{1}{\Gamma|\Omega| + \rho_s k^2}$. As one may readily verify, this integral converges in the infrared, and therefore, the fluctuations do not destroy the ordering (unlike the case of a non-dissipative chain where the analogous correction to the order parameter diverges logarithmically).

We note that the same conclusion as above can also be reached by a semiclassical, large- S calculation using the Holstein-Primakoff representation for spins. Details can be found in the supplemental material of Ref. 17.

MEAN-FIELD THEORY FOR A DISSIPATIVE SPIN CHAIN KONDO COUPLED TO 2D ELECTRONS

To formulate the mean field we consider a spin-1/2 chain along the x -axis of a square conducting substrate and impose periodic boundary conditions both along the spin chain and on the substrate. In this case the unit cell \mathbf{r} contains the $n = 1 \cdots L$ conduction electrons $\hat{c}_{\mathbf{r},n,\sigma}$ and a single spin-1/2 degree of freedom $\hat{S}_{\mathbf{r}}$. We use the fermionic representation of local moment $\hat{S}_{\mathbf{r}} = \frac{1}{2} \sum_{\sigma,\sigma'} \hat{d}_{\mathbf{r},\sigma}^\dagger \boldsymbol{\sigma}_{\sigma,\sigma'} \hat{d}_{\mathbf{r},\sigma'}$ and impose the constraint $\sum_{\sigma} \hat{d}_{\mathbf{r},\sigma}^\dagger \hat{d}_{\mathbf{r},\sigma} = 1$.

In this fermionic representation the partition function Z for the Hamiltonian given in Eq. (1) of main paper can be written as,

$$Z = \text{Tr}[e^{-\beta \hat{H}}] \equiv \int \mathcal{D}(\bar{\phi}, \phi, \lambda) e^{-\mathcal{S}(\bar{\phi}, \phi, \lambda)} \quad (\text{S12})$$

with $\phi = (c, d)$ and the action $\mathcal{S}(\bar{\phi}, \phi, \lambda)$,

$$\begin{aligned} \mathcal{S}(\bar{\phi}, \phi, \lambda) = & \int_0^\beta d\tau \sum_{\mathbf{r},n,\sigma} \bar{c}_{\mathbf{r},n,\sigma,\tau} \partial_\tau c_{\mathbf{r},n,\sigma,\tau} - t \int_0^\beta d\tau \sum_{\mathbf{r},n,\sigma} (\bar{c}_{\mathbf{r},n,\sigma,\tau} c_{\mathbf{r},n+1,\sigma,\tau} + \bar{c}_{\mathbf{r},n,\sigma,\tau} c_{\mathbf{r}+\Delta\mathbf{r},n,\sigma,\tau} + \text{H.c}) \\ & - \frac{J_k}{4} \int_0^\beta d\tau \sum_{\mathbf{r},\sigma} (\bar{c}_{\mathbf{r},1,\sigma,\tau} d_{\mathbf{r},\sigma,\tau} + \text{H.c})^2 - \frac{J_h}{4} \int_0^\beta d\tau \sum_{\mathbf{r},\sigma} (\bar{d}_{\mathbf{r},\sigma,\tau} d_{\mathbf{r}+\Delta\mathbf{r},\sigma,\tau} + \text{H.c})^2 \\ & + \int_0^\beta d\tau \sum_{\mathbf{r},\sigma} \bar{d}_{\mathbf{r},\sigma,\tau} (\partial_\tau + i\lambda(\mathbf{r}, \tau)) d_{\mathbf{r},\sigma,\tau} - \int_0^\beta d\tau i\lambda(\mathbf{r}, \tau) \\ & - \Gamma \int_0^\beta d\tau \int_0^\beta d\tau' \sum_{\mathbf{r}} \left(\frac{1}{2} \sum_{\sigma,\sigma'} \bar{d}_{\mathbf{r},\sigma,\tau} \boldsymbol{\sigma}_{\sigma,\sigma'} d_{\mathbf{r},\sigma',\tau} \right) \chi^0(\mathbf{0}, \tau - \tau') \left(\frac{1}{2} \sum_{\sigma,\sigma'} \bar{d}_{\mathbf{r},\sigma,\tau'} \boldsymbol{\sigma}_{\sigma,\sigma'} d_{\mathbf{r},\sigma',\tau'} \right). \end{aligned} \quad (\text{S13})$$

In the above the summation $\sum_{\mathbf{r},n,\sigma}$ runs over the unit cell index $\mathbf{r} = 1 \cdots L$, the orbital index $n = 1 \cdots L$ and the z component of spin $\sigma = \uparrow (\downarrow)$. Furthermore, the scalar Lagrange multiplier $\lambda(\mathbf{r}, \tau)$ enforces the constraint and the last term corresponds to the dissipation where Γ is a dissipative coupling constant and $\chi^0(\mathbf{0}, \tau - \tau') \propto \frac{1}{(\tau - \tau')^2}$. Note that in Eq. (S13) the dissipation is added in an impromptu manner.

Next, we allow for the Kondo screening, the spinon hopping and the magnetic ordering along the spin chain with the following bond mean field decouplings,

$$V(\mathbf{r}, \tau) = \sum_{\sigma} \langle \bar{c}_{\mathbf{r},1,\sigma,\tau} d_{\mathbf{r},\sigma,\tau} \rangle = \sum_{\sigma} \langle \bar{d}_{\mathbf{r},\sigma,\tau} c_{\mathbf{r},1,\sigma,\tau} \rangle \quad (\text{S14})$$

$$\chi(\mathbf{r}, \tau) = \sum_{\sigma} \langle \bar{d}_{\mathbf{r},\sigma,\tau} d_{\mathbf{r}+\Delta\mathbf{r},\sigma,\tau} \rangle = \sum_{\sigma} \langle \bar{d}_{\mathbf{r}+\Delta\mathbf{r},\sigma,\tau} d_{\mathbf{r},\sigma,\tau} \rangle \quad (\text{S15})$$

$$m(\mathbf{r}, \tau) = \frac{1}{2} \sum_{\sigma} \langle \sigma \bar{d}_{\mathbf{r},\sigma,\tau} d_{\mathbf{r},\sigma,\tau} \rangle e^{-i\mathbf{Q}\cdot\mathbf{r}} = \frac{1}{2} \sum_{\sigma} \langle \sigma \bar{d}_{\mathbf{r},\sigma,\tau'} d_{\mathbf{r},\sigma,\tau'} \rangle e^{-i\mathbf{Q}\cdot\mathbf{r}}. \quad (\text{S16})$$

Here, \mathbf{Q} is the antiferromagnetic wave vector, $V(\mathbf{r}, \tau)$ is the hybridisation order parameter (or Higgs condensate) between c and d electrons, $\chi(\mathbf{r}, \tau)$ is the spinon hopping parameter along the spin chain and $m(\mathbf{r}, \tau)$ denotes the staggered magnetic order parameter along the z -direction.

The action of Eq. (S13) in terms of above mean-field order parameters can be written as,

$$\begin{aligned}
\mathcal{S}(\bar{\phi}, \phi, V, \chi, m, \lambda) = & \int_0^\beta d\tau \sum_{\mathbf{r}, n, \sigma} \bar{c}_{\mathbf{r}, n, \sigma, \tau} \partial_\tau c_{\mathbf{r}, n, \sigma, \tau} - t \int_0^\beta d\tau \sum_{\mathbf{r}, n, \sigma} (\bar{c}_{\mathbf{r}, n, \sigma, \tau} c_{\mathbf{r}, n+1, \sigma, \tau} + \bar{c}_{\mathbf{r}, n, \sigma, \tau} c_{\mathbf{r}+\Delta\mathbf{r}, n, \sigma, \tau} + \text{H.c.}) \\
& - \frac{J_k}{2} \int_0^\beta d\tau \sum_{\mathbf{r}, \sigma} V(\mathbf{r}, \tau) (\bar{c}_{\mathbf{r}, 1, \sigma, \tau} d_{\mathbf{r}, \sigma, \tau} + \text{H.c.}) - \frac{J_h}{2} \int_0^\beta d\tau \sum_{\mathbf{r}, \sigma} \chi(\mathbf{r}, \tau) (\bar{d}_{\mathbf{r}, \sigma, \tau} d_{\mathbf{r}+\Delta\mathbf{r}, \sigma, \tau} + \text{H.c.}) \\
& + \int_0^\beta d\tau \sum_{\mathbf{r}, \sigma} \bar{d}_{\mathbf{r}, \sigma, \tau} (\partial_\tau + i\lambda(\mathbf{r}, \tau)) d_{\mathbf{r}, \sigma, \tau} - \frac{\alpha}{2} \times \int_0^\beta d\tau \sum_{\mathbf{r}, \sigma} m(\mathbf{r}, \tau) (\sigma \bar{d}_{\mathbf{r}, \sigma, \tau} d_{\mathbf{r}+\mathbf{Q}, \sigma, \tau} + \text{H.c.}) \\
& + \int_0^\beta d\tau \sum_{\mathbf{r}} \left(\frac{J_k}{2} |V(\mathbf{r}, \tau)|^2 + \frac{J_h}{2} |\chi(\mathbf{r}, \tau)|^2 + \alpha |m(\mathbf{r}, \tau)|^2 - i\lambda(\mathbf{r}, \tau) \right). \tag{S17}
\end{aligned}$$

In the above α denotes the renormalised dissipative coupling, $\alpha \propto \Gamma \int d\tau \frac{1}{\tau^2}$.

To find the saddle-point solutions,

$$\frac{d\mathcal{S}(\bar{\phi}, \phi, V, \chi, m, \lambda)}{dV(\mathbf{r}, \tau)} = 0, \quad \frac{d\mathcal{S}(\bar{\phi}, \phi, V, \chi, m, \lambda)}{d\chi(\mathbf{r}, \tau)} = 0, \quad \frac{d\mathcal{S}(\bar{\phi}, \phi, V, \chi, m, \lambda)}{dm(\mathbf{r}, \tau)} = 0, \quad \frac{d\mathcal{S}(\bar{\phi}, \phi, V, \chi, m, \lambda)}{d\lambda(\mathbf{r}, \tau)} = 0 \tag{S18}$$

we restrict the search to space- and time-independent mean-field order parameters; $V(\mathbf{r}, \tau) = V$, $\chi(\mathbf{r}, \tau) = \chi$, $m(\mathbf{r}, \tau) = m$ and enforces the constraint on average $\lambda(\mathbf{r}, \tau) = \lambda$. Hence, from now onward we will work in the Hamiltonian formalism with static mean-field order parameters.

The mean-field Hamiltonian can be written as,

$$\begin{aligned}
\hat{H}_{mf} = & -t \sum_{\mathbf{r}, n, \sigma} (\hat{c}_{\mathbf{r}, n, \sigma}^\dagger \hat{c}_{\mathbf{r}, n+1, \sigma} + \hat{c}_{\mathbf{r}, n, \sigma}^\dagger \hat{c}_{\mathbf{r}+\Delta\mathbf{r}, n, \sigma} + \text{H.c.}) - \frac{J_k V}{2} \sum_{\mathbf{r}, \sigma} (\hat{c}_{\mathbf{r}, 1, \sigma}^\dagger \hat{d}_{\mathbf{r}, \sigma} + \text{H.c.}) \\
& - \frac{J_h \chi}{2} \sum_{\mathbf{r}, \sigma} (\hat{d}_{\mathbf{r}, \sigma}^\dagger \hat{d}_{\mathbf{r}+\Delta\mathbf{r}, \sigma} + \text{H.c.}) + \lambda \sum_{\mathbf{r}, \sigma} \hat{d}_{\mathbf{r}, \sigma}^\dagger \hat{d}_{\mathbf{r}, \sigma} - \frac{\alpha m}{2} \sum_{\mathbf{r}, \sigma} (\sigma \hat{d}_{\mathbf{r}, \sigma}^\dagger \hat{d}_{\mathbf{r}+\mathbf{Q}, \sigma} + \text{H.c.}) + N_u e_0 \tag{S19}
\end{aligned}$$

with, $e_0 = (\frac{J_k V^2}{2} + \frac{J_h \chi^2}{2} + \alpha m^2 - \lambda)$ and N_u is the number of unit cells. Hereafter, we set $\lambda = 0$ for a particle-hole-symmetric band.

Further, using the Fourier transforms,

$$\hat{c}_{\mathbf{r}, n, \sigma} = \frac{1}{\sqrt{N_u/2}} \sum_{\mathbf{k} \in \text{MBZ}} e^{i\mathbf{k} \cdot \mathbf{r}} \hat{c}_{\mathbf{k}, n, \sigma}, \quad \hat{d}_{\mathbf{r}, \sigma} = \frac{1}{\sqrt{N_u/2}} \sum_{\mathbf{k} \in \text{MBZ}} e^{i\mathbf{k} \cdot \mathbf{r}} \hat{d}_{\mathbf{k}, \sigma} \tag{S20}$$

the mean-field Hamiltonian in momentum space can be written as,

$$\hat{H}_{mf} = \sum_{\mathbf{k} \in \text{MBZ}, n, \sigma} \hat{\phi}_{\mathbf{k}, n, \sigma}^\dagger M(\mathbf{k}) \hat{\phi}_{\mathbf{k}, n, \sigma} + N_u e_0 \tag{S21}$$

with $\hat{\phi}_{\mathbf{k}, n, \sigma}^\dagger = (\hat{c}_{\mathbf{k}, 1, \sigma}^\dagger, \hat{c}_{\mathbf{k}+\mathbf{Q}, 1, \sigma}^\dagger, \hat{c}_{\mathbf{k}, 2, \sigma}^\dagger, \hat{c}_{\mathbf{k}+\mathbf{Q}, 2, \sigma}^\dagger, \hat{c}_{\mathbf{k}, 3, \sigma}^\dagger, \hat{c}_{\mathbf{k}+\mathbf{Q}, 3, \sigma}^\dagger, \dots, \hat{c}_{\mathbf{k}, L, \sigma}^\dagger, \hat{c}_{\mathbf{k}+\mathbf{Q}, L, \sigma}^\dagger, \hat{d}_{\mathbf{k}, \sigma}^\dagger, \hat{d}_{\mathbf{k}+\mathbf{Q}, \sigma}^\dagger)$ and

$M(\mathbf{k}) =$

$$\begin{pmatrix}
-2t \cos \mathbf{k} & 0 & -t & 0 & 0 & 0 & \dots & -t & 0 & \frac{-J_k V}{2} & 0 \\
0 & 2t \cos \mathbf{k} & 0 & -t & 0 & 0 & \dots & 0 & -t & 0 & \frac{-J_k V}{2} \\
-t & 0 & -2t \cos \mathbf{k} & 0 & -t & 0 & \dots & 0 & 0 & 0 & 0 \\
0 & -t & 0 & 2t \cos \mathbf{k} & 0 & -t & \dots & 0 & 0 & 0 & 0 \\
0 & 0 & -t & 0 & -2t \cos \mathbf{k} & 0 & \dots & 0 & 0 & 0 & 0 \\
0 & 0 & 0 & -t & 0 & 2t \cos \mathbf{k} & \dots & 0 & 0 & 0 & 0 \\
0 & 0 & 0 & 0 & -t & 0 & \dots & 0 & 0 & 0 & 0 \\
\dots & \dots & \dots & \dots & \dots & \dots & \dots & \dots & \dots & \dots & \dots \\
-t & 0 & 0 & 0 & 0 & 0 & \dots & -2t \cos \mathbf{k} & 0 & 0 & 0 \\
0 & -t & 0 & 0 & 0 & 0 & \dots & 0 & 2t \cos \mathbf{k} & 0 & 0 \\
\frac{-J_k V}{2} & 0 & 0 & 0 & 0 & 0 & \dots & 0 & 0 & -J_h \chi \cos \mathbf{k} & \frac{-\alpha m \sigma}{2} \\
0 & \frac{-J_k V}{2} & 0 & 0 & 0 & 0 & \dots & 0 & 0 & \frac{-\alpha m \sigma}{2} & J_h \chi \cos \mathbf{k}
\end{pmatrix}.$$

Diagonalizing the mean-field Hamiltonian, $U^\dagger(\mathbf{k})M(\mathbf{k})U(\mathbf{k}) = \text{Diag}(E_{\mathbf{k},1}, \dots, E_{\mathbf{k},2(L+1)})$ gives:

$$\hat{H}_{mf} = N_u e_0 + \sum_{\mathbf{k} \in \text{MBZ}, n, \sigma} E_{\mathbf{k},n,\sigma} \hat{\gamma}_{\mathbf{k},n,\sigma}^\dagger \hat{\gamma}_{\mathbf{k},n,\sigma}. \quad (\text{S22})$$

Here, the \mathbf{k} summation goes over the reduced magnetic Brillouin zone (MBZ) and $\hat{\gamma}_{\mathbf{k}}^\dagger = \hat{\phi}_{\mathbf{k}}^\dagger U(\mathbf{k})$.

Fig. S1 plots the mean-field order parameters V , χ , and m as a function of Kondo coupling. Specifically, by fixing $\alpha/t = 2$ and $J_h/t = 1$, the mean-field theory gives the two phases, (i) a dissipation-induced magnetically ordered phase characterized by $m = 1, V = 0, \chi = 0$ and (ii) a disordered Kondo-screened phase characterized by $m = 0, V \neq 0, \chi \neq 0$.

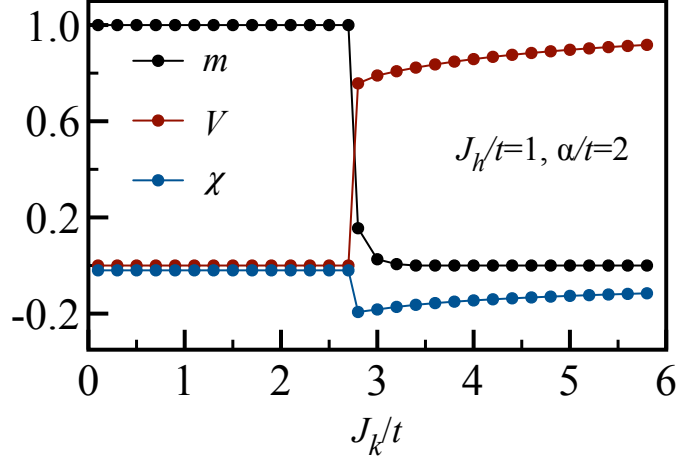


FIG. S1. Mean-field order parameters as a function of J_k/t at $N_u = L_x = L_y = L = 100$.

Further, to explore heavy-Fermi-liquid properties at large J_k limit we set $\alpha = 0$ in Eq. (S21) and self consistently search for mean-field order parameters V and χ in the Brillouin zone (BZ). In this case for $J_k/t < 2$ we observe a Kondo-breakdown phase and for $J_k/t \gtrsim 2$ a transition into the Kondo-screened phase. Considering that the Kondo-breakdown phase is an artefact of the mean-field approach in the following we only focus on the Kondo-screened paramagnetic phase.

Fig. S2 plots the mean-field results for equal-time spin-spin correlation function $C(\mathbf{r}, 0) = \frac{1}{L} \sum_{\mathbf{q}} e^{i(\mathbf{q}+\mathbf{Q}) \cdot \mathbf{r}} \langle \hat{S}^z(\mathbf{q}, 0) \hat{S}^z(-\mathbf{q}, 0) \rangle$ along the spin chain as a function of r at $J_k/t = 3$ and $J_k/t = 4$. Here, the spins acquire the $1/r^4$ power law decay of 2D conduction electrons. Correspondingly, Fig. S3 plots the time displaced spin-spin correlation function $C(\mathbf{0}, \tau) = \frac{1}{L} \sum_{\mathbf{q}} \langle T_\tau \hat{S}^z(\mathbf{q}, 0) \hat{S}^z(-\mathbf{q}, \tau) \rangle$ as a function of imaginary time τ . Here, the spins acquire the $1/\tau^2$ power-law decay of 2D conduction electrons.

To understand the heavy band in the composite-fermion spectral function $A_\psi(k, \omega)$ (see Figs. 7 (a) and (b) of the main paper) we compute the retarded Green functions $G_d^{\text{ret}}(\mathbf{k}, \omega)$ and $G_c^{\text{ret}}(\mathbf{k}, \omega)$ on d electrons and the c electrons respectively as given below,

$$G_d^{\text{ret}}(\mathbf{k}, \omega) = -i \int_0^\infty dt e^{i\omega t} \sum_{\sigma} \langle \{ \hat{d}_{\mathbf{k},\sigma}(t), \hat{d}_{\mathbf{k},\sigma}^\dagger(0) \} \rangle = \sum_n \frac{|U_{\mathbf{k},L+1,n}|^2}{\omega - E_{\mathbf{k},n} + i0^+} \quad (\text{S23})$$

$$G_c^{\text{ret}}(\mathbf{k}, \omega) = -i \int_0^\infty dt e^{i\omega t} \sum_{\sigma} \langle \{ \hat{c}_{\mathbf{k},1,\sigma}(t), \hat{c}_{\mathbf{k},1,\sigma}^\dagger(0) \} \rangle = \sum_n \frac{|U_{\mathbf{k},1,n}|^2}{\omega - E_{\mathbf{k},n} + i0^+}. \quad (\text{S24})$$

Fig. S4 plots the d -spectral function $A_d(\mathbf{k}, \omega) = -\frac{1}{\pi} \text{Im} G_d^{\text{ret}}(\mathbf{k}, \omega)$ as a function of energy and momentum in the Kondo-screened phase. Similarly, Fig. S5 plots the spectral function of the Kondo-coupled row of conduction electrons $A_c(\mathbf{k}, \omega) = -\frac{1}{\pi} \text{Im} G_c^{\text{ret}}(\mathbf{k}, \omega)$. As apparent, in $A_d(\mathbf{k}, \omega)$, we observe a band that detaches from the continuum and that is reminiscent of the heavy fermion band observed within a one-dimensional Kondo insulator [45]. This heavy-fermion state hybridizes with the other conduction electrons. The notion of heavy Fermi liquid for this dimensional-mismatch Kondo problem becomes precise when considering the volume of the Fermi surface as described by Luttinger's theorem, discussed in the next section.

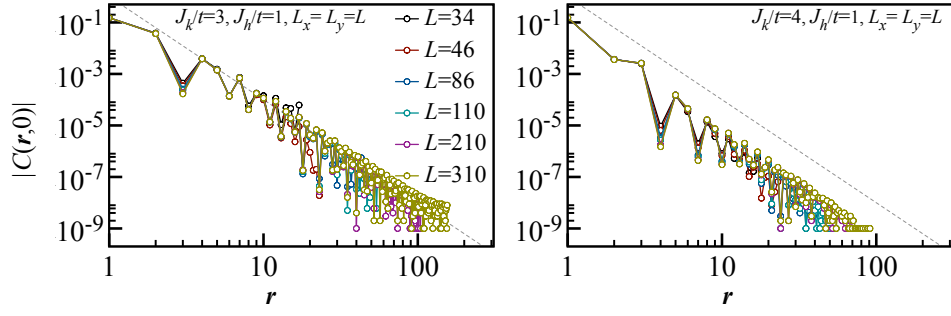


FIG. S2. Equal-time spin-spin correlation function $|C(\mathbf{r}, 0)|$ along the spin chain with respect to distance r in the Kondo-screened phase within the mean-field calculation. The dashed grey line represents the $1/r^4$ power law.

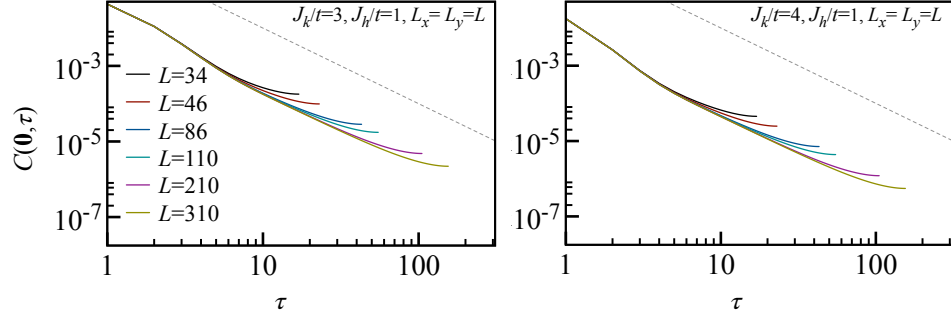


FIG. S3. Time-displaced spin-spin correlation function $C(\mathbf{0}, \tau)$ along the spin chain with respect to imaginary τ in the Kondo-screened phase within the mean-field calculation. The dashed grey line represents the $1/\tau^2$ power law.

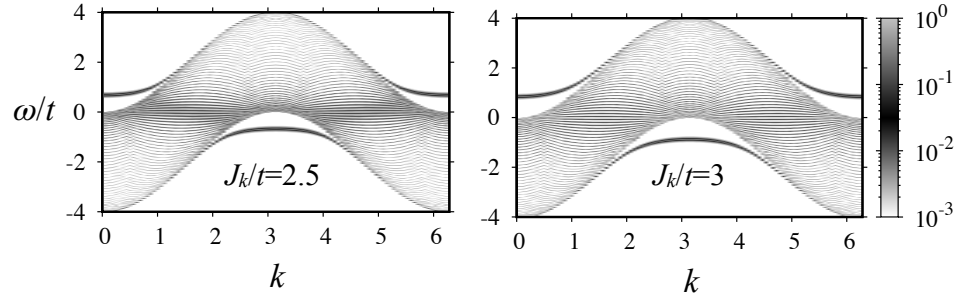


FIG. S4. The d spectral function $A_d(k, \omega)$ as a function of energy ω/t and momentum k at $J_h/t = 1$ obtained within the mean-field calculation.

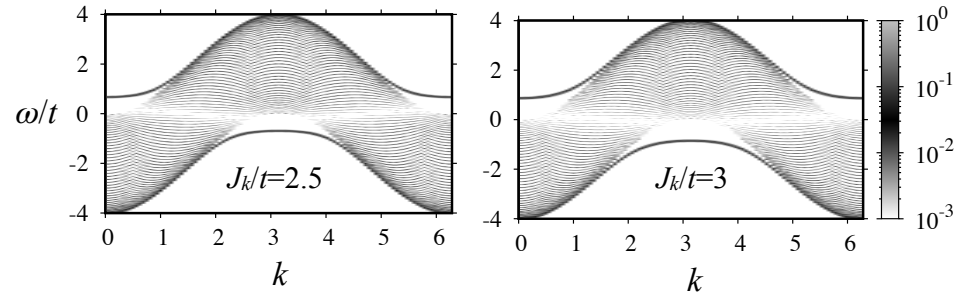


FIG. S5. The c spectral function $A_c(k, \omega)$ as a function of energy ω/t and momentum k at $J_h/t = 1$ obtained within the mean-field calculation.

LUTTINGER THEOREM FOR A HYBRID-DIMENSIONALITY KONDO LATTICE MODEL

In Ref. 44, Oshikawa showed that if the low-energy theory of a standard Kondo lattice model is a conventional Fermi liquid, then the volume of the Fermi surface equals the sum of the density of the conduction electrons and density of the local moments (mod 2), i.e., the Fermi surface is ‘large’. Here we discuss Oshikawa’s argument in the context of our model, or more generally, in the context of models where the conduction electrons and the local moments have a dimensional mismatch. This allows one to give a precise meaning to the heavy Fermi liquid phase in such models.

Consider our model defined in Eq. (1) of the main paper with local moments that are located along a chain at $y = 0$. We put this system on a $L_x \times L_y$ cylinder with periodic boundary condition along the x direction, and denote by ν_σ the density of conduction electrons with spin $\sigma = \uparrow, \downarrow$, i.e., $\nu_\sigma = \langle \sum_i c_{i\sigma}^\dagger c_{i\sigma} \rangle / (L_x L_y)$. This system can be thought of as a translationally invariant one-dimensional system where each unit cell contains a single local moment with spin-1/2, and $L_y \nu_\sigma$ conduction electrons with spin σ . We now adiabatically insert a 2π flux of a gauge field that only couples to say, up-spin electrons. Let us denote the original Hamiltonian as $H(\Phi = 0)$ and the final Hamiltonian as $H(\Phi = 2\pi)$. If the original ground state $|\psi(\Phi = 0)\rangle$ has lattice momentum p_{0x} , and eigenenergy E_0 , then after this adiabatic evolution, it will evolve to a new state $|\psi(\Phi = 2\pi)\rangle$ with the same lattice momentum p_{0x} and, same eigenenergy E_0 i.e. $H(\Phi = 2\pi)|\psi(\Phi = 2\pi)\rangle = E_0|\psi(\Phi = 2\pi)\rangle$. However, $H(0) \neq H(2\pi)$ and in fact $U_\uparrow^\dagger H(\Phi = 2\pi) U_\uparrow = H(\Phi = 0)$ where $U_\uparrow = e^{\frac{2\pi i}{L_x} \sum_x x (n_\uparrow(x) + S^z(x))}$ and $n_\uparrow(x) = \sum_{y=1}^{L_y} c_{x,y,\uparrow}^\dagger c_{x,y,\uparrow}$. Now one may use the commutation relation between the translational operator T_x and U_\uparrow to show that the state $U_\uparrow |\psi(\Phi = 2\pi)\rangle$ carries momentum $p_{0x} + 2\pi(\nu_\uparrow L_y + 1/2)$ where we have assumed that the magnetization of the local moments is zero. If the low-energy theory is a Fermi liquid, the insertion of 2π flux shifts the Fermi surface of the up-spin quasiparticles by momentum $2\pi/L_x$, and therefore, the momentum transferred also equals $\frac{2\pi}{L_x} \times N_\uparrow^{L_x}$ where $N_\uparrow^{L_x}$ is the number of occupied momentum modes for the up-spin quasiparticles. Equating the two expressions for the momentum transferred, one finds $N_\uparrow^{L_x} = (\nu_\uparrow L_y + 1/2)L_x$. If the system did not have any local moments, then this same procedure would instead yield $N_\uparrow^{L_x} = \nu_\uparrow L_y L_x$. The additional ‘+1/2’ inside the brackets in the expression for $N_\uparrow^{L_x}$ provides a precise meaning to the statement that the local moments are absorbed in the Fermi volume. One may run the same argument for the down-spin electrons, and obtain $N_\uparrow^{L_x} + N_\downarrow^{L_x} = (\nu L_y + 1)L_x$ where $\nu = \nu_\uparrow + \nu_\downarrow$ is the total density of conduction electrons. More generally, this equation provides a non-perturbative definition of the heavy Fermi liquid state for a mixed-dimensionality model such as ours.

SPIN-1/2 XXZ CHAIN ON A 2D METAL

The Hamiltonian for a spin-1/2 XXZ chain on a 2D metal can be written as

$$\hat{H} = -t \sum_{\langle i,j \rangle} (\hat{c}_i^\dagger \hat{c}_j + \text{H.c.}) + \frac{J_k}{2} \sum_{r=1}^L \hat{c}_r^\dagger \sigma \hat{c}_r \cdot \hat{S}_r + \sum_{r=1}^L \left(\frac{J^\perp}{2} (\hat{S}_r^+ \hat{S}_{r+\Delta r}^- + \hat{S}_r^- \hat{S}_{r+\Delta r}^+) + J^z \hat{S}_r^z \hat{S}_{r+\Delta r}^z \right) \quad (\text{S25})$$

where J^\perp and J^z are the transverse and longitudinal exchange couplings along the spin chain.

The space and time displaced spin-spin correlation power-law decays along the decoupled XXZ spin chain are set by the Luttinger parameter $K = \left[\frac{2}{\pi} \cos^{-1}(-J^z/J^\perp) \right]^{-1}$ [46]. Specifically, the transverse and longitudinal spin-spin correlation functions are given by the power-law decays

$$\chi^\perp(\mathbf{r}, \tau) = e^{i\mathbf{Q}\cdot\mathbf{r}} \langle \hat{S}^+(\mathbf{r}, \tau) \hat{S}^-(0, 0) \rangle \propto \frac{1}{\sqrt{(v_s \tau)^2 + r^2}^{1/2K}} \quad (\text{S26})$$

$$\chi^z(\mathbf{r}, \tau) = e^{i\mathbf{Q}\cdot\mathbf{r}} \langle \hat{S}^z(\mathbf{r}, \tau) \hat{S}^z(0, 0) \rangle \propto \frac{1}{\sqrt{(v_s \tau)^2 + r^2}^{2K}} \quad (\text{S27})$$

with v_s being the spin velocity. The case $K = 1/2$ corresponds to the isotropic Heisenberg point $J^\perp = J^z$ where the power-law decay takes the form $1/\sqrt{(v_s \tau)^2 + r^2}$. The regime $K > 1/2$ corresponds to an anisotropic XXZ chain with $J^\perp > J^z$.

In power counting for $K > 1/2$ the Kondo coupling is relevant and irrelevant with respect to the scaling dimensions of transverse and longitudinal spin components. Hence one can expect to see a stronger tendency towards dissipation-induced ordering in the transverse correlations along the XXZ chain. To check this point of view we have performed our QMC simulation at $J^\perp = 4J^z$. This choice of anisotropy is motivated by Co adatoms on $\text{Cu}_2\text{N}/\text{Cu}(100)$ surface [1].

Specifically, we focus on the transverse R^\perp and longitudinal R^z components of the correlation ratio,

$$R^\perp = 1 - \frac{\chi^\perp(\mathbf{Q} - \delta\mathbf{k}, 0)}{\chi^\perp(\mathbf{Q}, 0)}, \quad R^z = 1 - \frac{\chi^z(\mathbf{Q} - \delta\mathbf{k}, 0)}{\chi^z(\mathbf{Q}, 0)}. \quad (\text{S28})$$

Fig. S6 (a) and (b) plots R^\perp and R^z as a function of J_k/t . Clearly as a function of J_k/t the transverse correlation ratio R^\perp reveals a quantum critical point at $J_k^c/t \sim 2.3$. Noticeably, the enhancement in R^\perp with increasing L is more pronounced for $J_k \lesssim 2$ as compared to Fig. 2(b) of the main paper. In contrast, the longitudinal part R^z does not show any critical behavior.

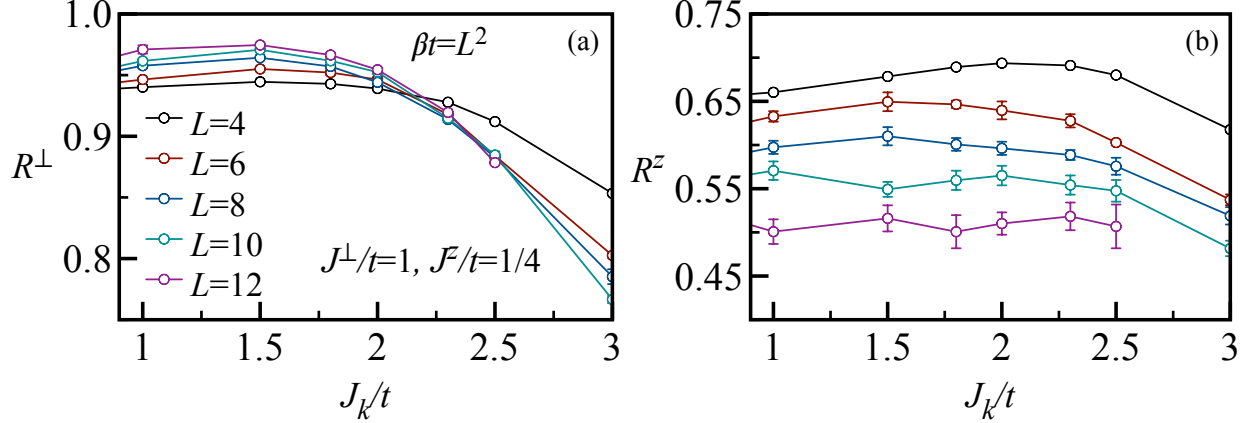


FIG. S6. QMC results for a spin-1/2 XXZ chain on a 2D metal at $J^\perp = 4J^z$. Here, the Luttinger parameter reads $K = 0.861429$. Left: Transverse component of correlation ratio R^\perp as a function of J_k/t at $\beta t = L^2$. Right: Longitudinal component of correlation ratio R^z as a function of J_k/t at $\beta t = L^2$.

FURTHER QMC RESULTS

In this section we present supplemental QMC results supporting the interpretation in the main paper. In Fig. S7 we present the equal time spin-spin correlations as a function of size and temperature. In the Heisenberg limit, $J_k = 0$, the dynamical exponent reads $z = 1$ such that system sizes $\beta \propto L$ suffice to access ground-state properties. Upon inspection we see practically no difference in the data when considering $\beta t = L$, $\beta t = 2L$, and $\beta t = 3L$. In the vicinity of the quantum phase transition, $J_k/t = 2$, we see that since $z \simeq 2$ the choice $\beta t = L$ results in high temperature data. In particular at $\beta t = L$ we see that the spin-spin correlations decay quicker than $1/r$ and we ultimately expect to see an exponential decay in the large-size limit. This exponential decay stems from thermal fluctuations.

In Fig. S8 we consider the imaginary decay. Consider the $L = 44$ lattice as a function of temperature, as shown in the insets. Lowering the temperature for the Heisenberg case shows that one quickly resolves the finite size gap given by $1/L$. Beyond this scale, the imaginary-time data falls off exponentially. In contrast in the vicinity of the critical point as well as in the crossover dissipative phase, we do not seem to be able to resolve the finite-size gap. In fact, in the vicinity of the critical point, we expect it to scale as $1/L^z$ with $z = 2$.

Figs. S9 and S10 plot the same data as in Fig. 4 of the main text but at $\beta t = L^2/2$ and $\beta t = L^2/4$. For $\beta t = L^2/4$ we can reach larger system sizes and the same overall conclusions hold. Fig. S11 plots the correlation ratio, R , as a function of system size but for various aspect ratios, $\beta t = L^2$, $\beta t = L^2/2$ and $\beta t = L^2/4$ as well as as a function of J_k/t . Choosing the aspect ratio $\beta t = L^2/4$ allows us to reach larger lattices. As apparent, the data is consistent with a slow increase of R below J_k^c/t . This behavior is characteristic of the crossover regime, where the lattice sizes are not large enough to unambiguously detect long range antiferromagnetic ordering. Figs. S12 (a) and (b) plot the momentum-integrated composite fermion spectral function $A_\psi(\omega)$ as a function of energy ω/t in ordered and disordered phases, respectively.

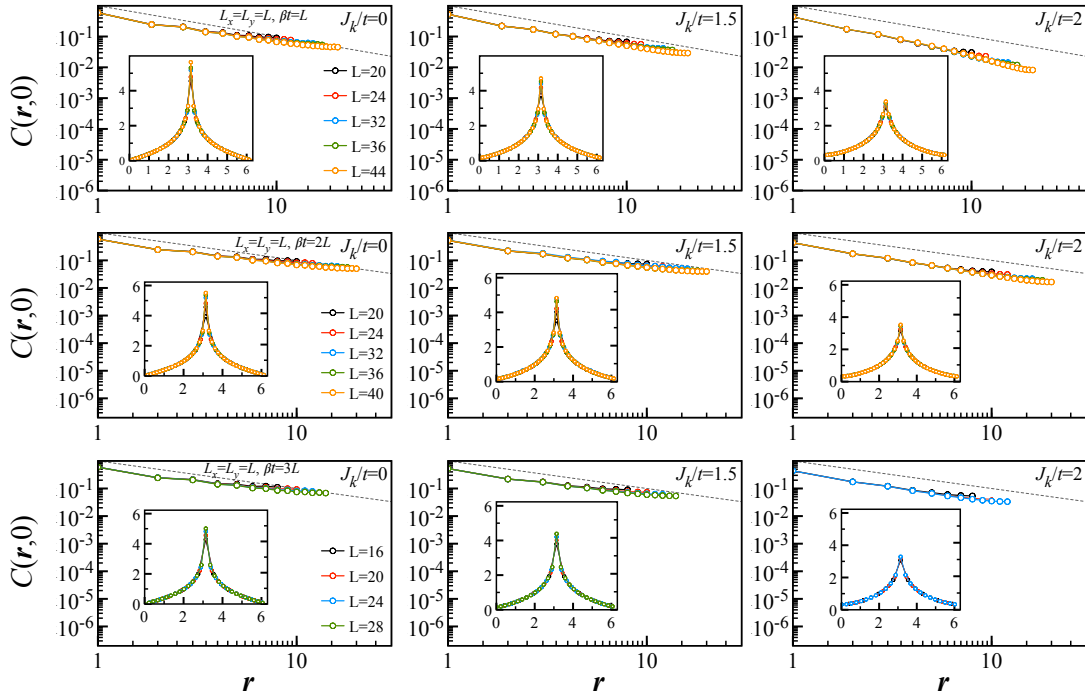


FIG. S7. Same as Fig. 4 (a)-(c) of the main paper on larger system sizes at $\beta t = L, 2L, 3L$ in the ordered phase. Equal-time spin-spin correlation function $C(\mathbf{r}, 0)$ with respect to distance r at $J_h/t = 1$ for given J_k/t values. Top row, $\beta t = L$. Middle row, $\beta t = 2L$. Bottom row, $\beta t = 3L$. The dashed grey line denotes the $1/r$ power law. The insets plots corresponding static spin structure factor $S(k)$ with respect to momentum vector k .

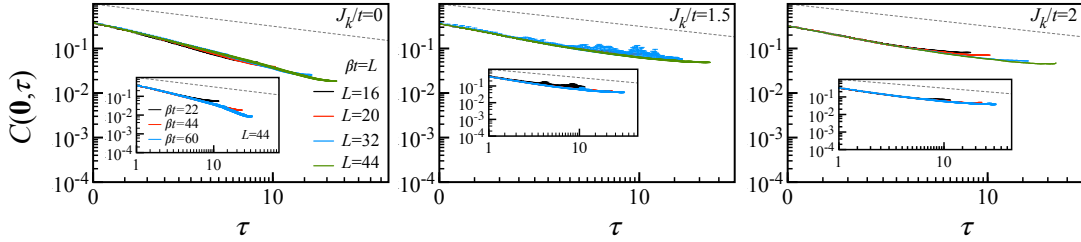


FIG. S8. Same as Fig. 4 (b)-(d) of the main paper on larger system sizes at $\beta t = L$ in the ordered phase. Time-displaced spin-spin correlation function $C(\mathbf{0}, \tau)$ with respect to imaginary time τ at $\beta t = L, J_h/t = 1$. Left, $J_k/t = 0$. Middle, $J_k/t = 1.5$. Right, $J_k/t = 2$. The dashed grey line denotes the $1/\sqrt{\tau}$ power law. The insets plot the same at a fixed $L = 44$ for given inverse temperatures βt .

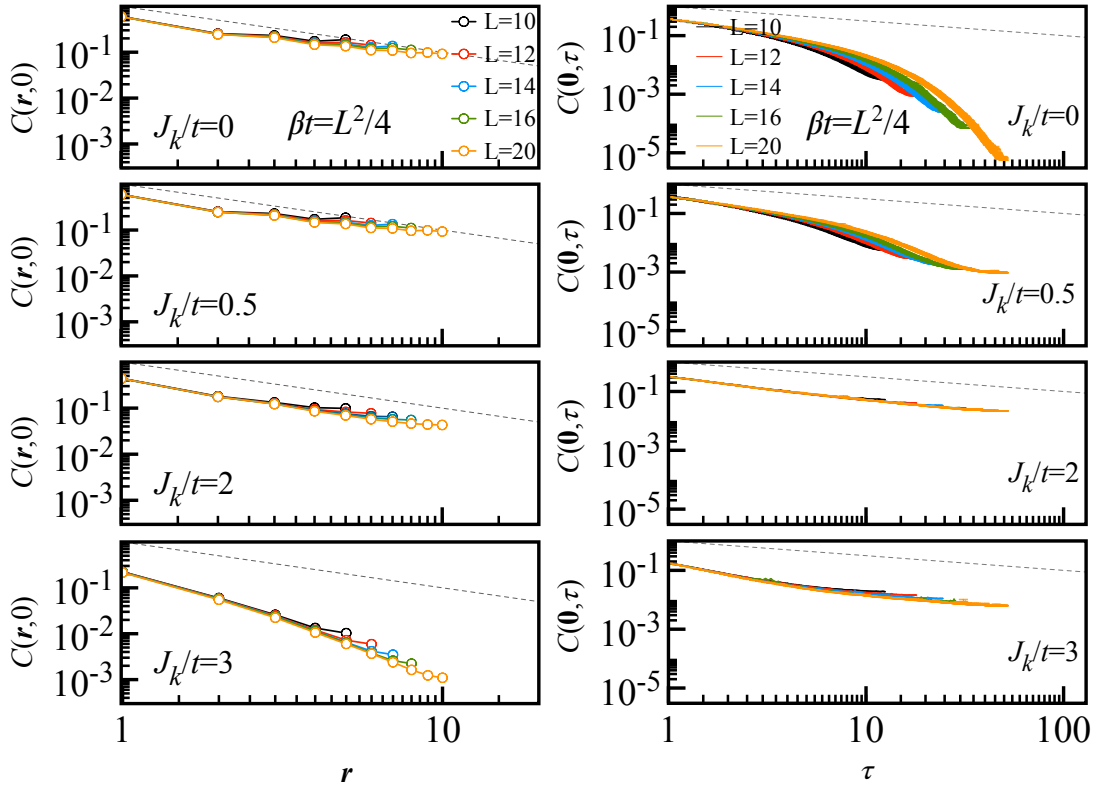


FIG. S9. Same as Fig. 4 of the main paper at $\beta t = L^2/4$ and $J_h/t = 1$ for given J_k/t values. Left: Equal-time correlations $C(r,0)$ with respect to distance r . Here, the dashed grey lines denote the $1/r$ power law. Right: Time-displaced correlations $C(0,\tau)$ with respect to imaginary time τ . Here, the dashed grey lines denote the $1/\sqrt{\tau}$ power law.

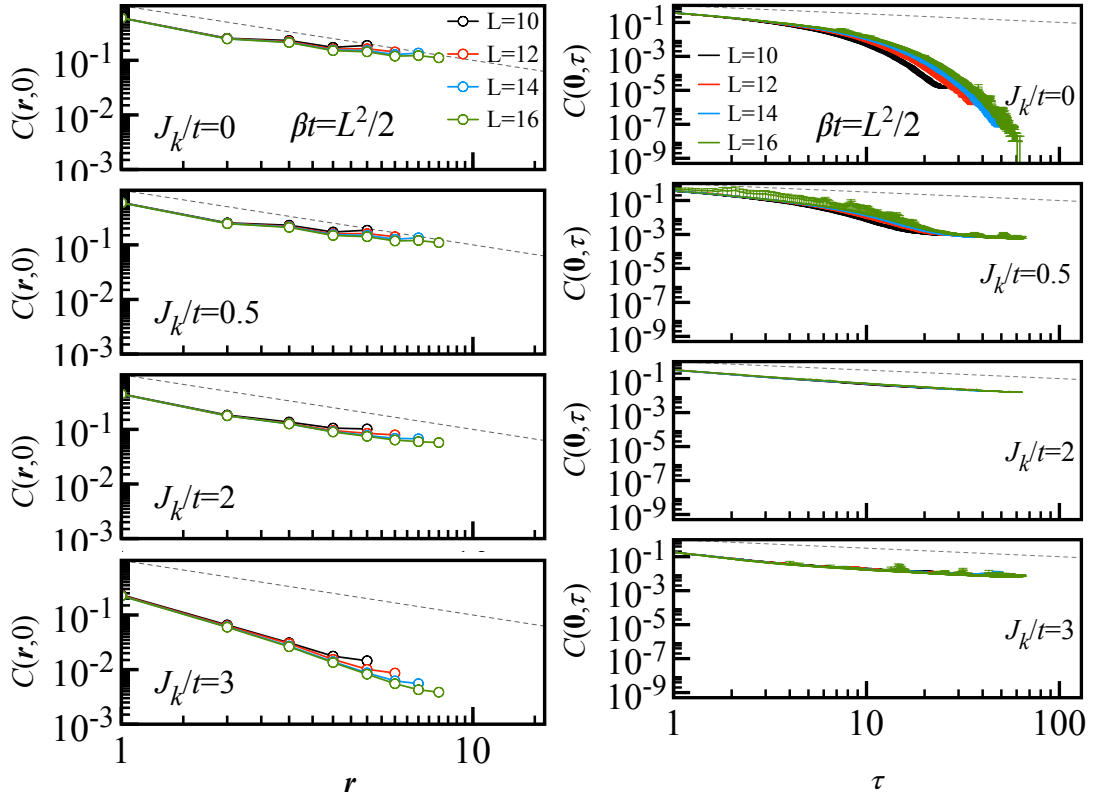


FIG. S10. Same as Fig. 4 of the main paper at $\beta t = L^2/2$ and $J_h/t = 1$ for given J_k/t values. Left: Equal-time correlations $C(r,0)$ with respect to distance r . Here, the dashed grey lines denote the $1/r$ power law. Right: Time-displaced correlations $C(0,\tau)$ with respect to imaginary time τ . Here, the dashed grey lines denote the $1/\sqrt{\tau}$.

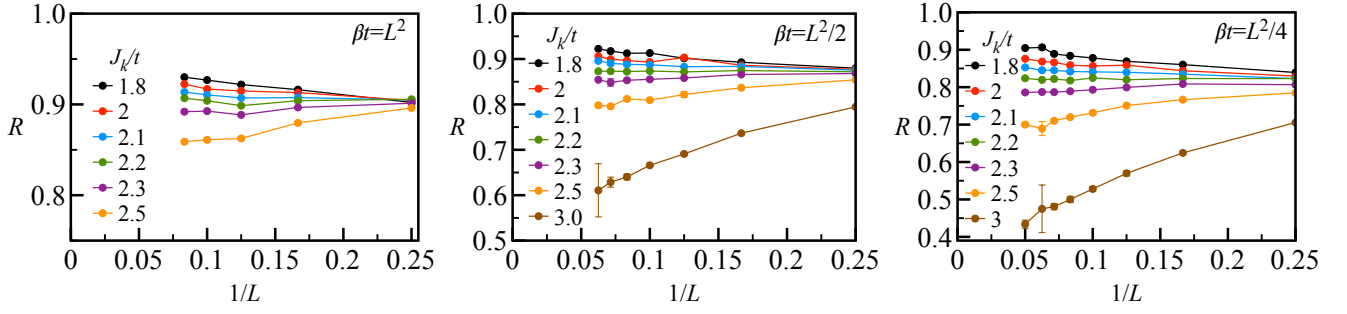


FIG. S11. Left: Correlation ratio R as a function of $1/L$ at $\beta t = L^2$, $J_h/t = 1$ for given J_k/t values. Middle: Same at $\beta t = L^2/2$. Right: Same at $\beta t = L^2/4$.

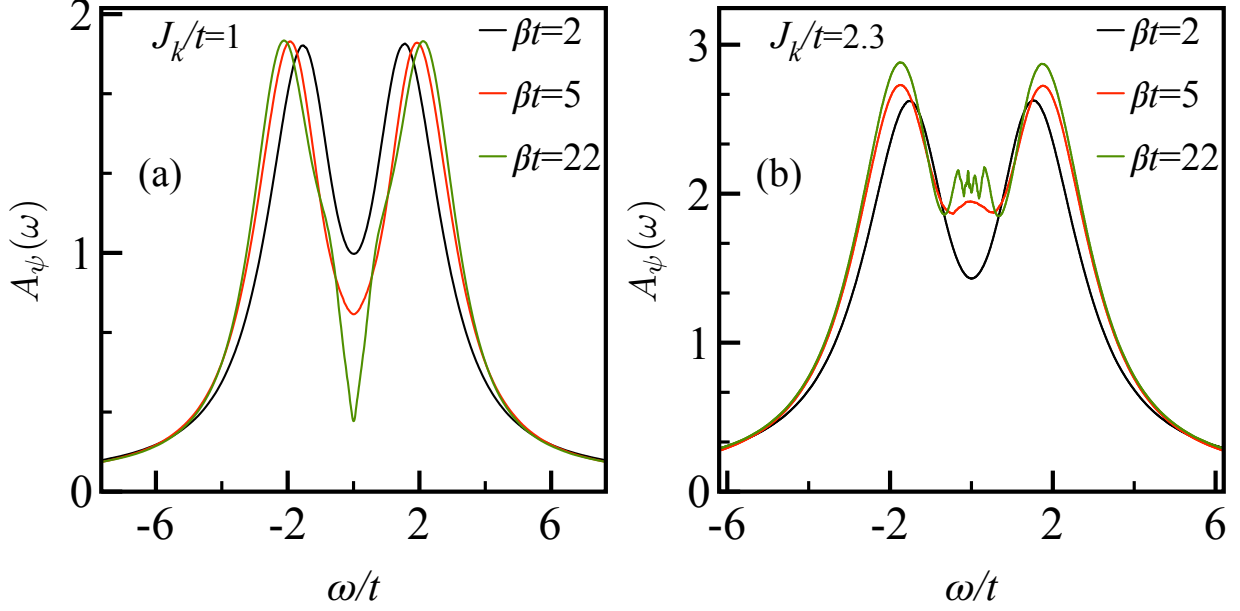


FIG. S12. Local, i.e. momentum-integrated, composite-fermion spectral function $A_\psi(\omega)$ as a function of energy ω/t at $L = L_x = L_y = 44$, $J_h/t = 1$. (a) In the ordered phase at $J_k/t = 1$ and (b) in the paramagnetic phase at $J_k/t = 2.3$.